國立交通大學

顯示科技研究所

碩士論文

# 動態式 OFDM 調變與 60-GHz 光載微波無線訊號系統

# Dynamic OFDM Modulation in 60 GHz RoF System with Wireless Transmission

研 究 生：王何立穎

指導教授：陳智弘 教授

中華民國九十九年八月

# Dynamic OFDM Modulation in 60 GHz RoF System with Wireless Transmission

By

Li-Ying Wang He

Thesis submitted to the Display Institute

College of Electrical Engineering and Computer Science

National Chiao Tung University

in partial fulfillment of the requirements

for the degree of Master in Display Institute

August 2010

## Abstract

Rapidly increasing demand for multi-Gbps wireless communication has attacted a lot of interest in the 7-GHz license-free spectrum at 60 GHz. Due to higher air-link loss at 60 GHz, the radio-over-fiber (RoF) system is a promising solution for extending the coverage of 60GHz wireless signals. However, 60 GHz wireless networking presents many technical challenges owing to the high carrier frequency and the wide channel bandwidth used. One of challenges is the non-flat channel response with up to 10 dB deviation within the 7 GHz spectrum.

In this thesis, bit-loading algorithm significantly improves performance and data throughput of ultra-wideband mm-wave RoF systems employing all-optical I/Q up-conversion architectures. By using bit-loading algorithm, we demonstrate bit-loading OFDM signal generation and transmission with a record of 32.65 Gb/s within 7-GHz license-free spectrum at 60 GHz band. Transmission over 25-km SMF transmission with negligible penalty is achieved without any dispersion compensation.

# 摘要

對於使用需求大量增長的 giga-bit 無線通信，在 60GHz 的 7GHz 的免授權頻段裡吸引了很多的興趣及研究。由於在 60GHz 這個頻段上，對於空氣傳輸有著非常大的衰減，於是透過 Radio-over-Fiber system 這樣的一個傳輸技術能夠有效的解決這樣的問題，然而，60GHz 無線網路仍然存在著許多技術上的挑戰，由於高載波頻率以及寬頻訊號的使用，會受到不平坦的通道響應所影響，而有著高達 10dB 多的偏差範圍，一個如此大的偏差值會導致 OFDM 訊號的每個副載波有著不同的雜訊比，如此一來每個副載波會有不同的傳輸效率。

在本篇論文裡，我們使用 Bit-loading 演算法去調校每個副載波已達到最佳的傳輸效率並且提升訊號的傳輸量。實驗結果成功的顯示出在 60GHz 的免授權 7GHz 頻段下，產生高達 32Gbps OFDM 訊號，在沒有任何色散補償的狀況下，經過 25 公里的單模光纖傳輸，此訊號幾乎沒有任何的損耗。

# Acknowledgements

在碩士班這兩年，首先感謝我的指導老師 陳智弘教授，提供良好的實驗環境以及無私的指導與照顧，讓我在碩士生涯中成長許多。實驗方面特別感謝林俊廷學長教導我許多實驗方法以及報告技巧，無私的指教與修正了我許多理論觀念，如果沒有學長如此的耐心指導下這篇論文無法如此順利的誕生，另外感謝施伯宗學長，江文智學長提供我許多實驗技巧以及在程式方面提供了我不少的幫助。

接下來要謝謝實驗室的伙伴：非常感謝芳銘學長以及嘉建學長還有已經畢業的而咨學姊、昱宏學長、漢昇學長和星宇學長在實驗上的幫助，另外謝謝彥霖陪伴我一起走過碩士班的生涯，還有學弟妹們，宜旻、維元、明義、俊鴻、冠穎及上詠在我實驗忙碌時，熱心地幫忙處理瑣事。 還要感謝平時給我許多鼓勵的好友們，謝謝你們的關心與支持。

最後要感謝我的家人，感謝你們的支持與鼓勵，並時時給予關心，讓我無後顧之憂的完成學業。

帶著愉快回憶和豐碩的收穫邁向下個新旅程，再會了交大。

王何立穎 于 風城 交大 民國九十九年九月

## CONTENTS

## List of Figures

# Chapter 1

# Introduction

## 1.1 Background

Due to the development in technology and science, people have much more demands for high-speed data transmission and high-quality images. In addition, some intelligent network devices, such as converged devices, smart phone, camera, GPS, and PDA, have been developed rapidly resulting in the huge need for internet service and the data transmission capacity for the network, and promoting the development in the wireless and wired network system.

In a society based on information technology, mobile phones, Wi-Fi and WiMAX become fundamental technology products. Additionally, it is more important to access information by wireless communication technology due to the fact that everyone wants to update or access information at any time. However, because of the constraints on the current commercial wireless communication bandwidth, the speed of wireless transmission for high-Definition images and data can't exceed in 1Gbit/s. Therefore, it is needed to raise the carrier frequency to solve the bandwidth limitations. Currently, the bandwidth is allowed to use in the USA as shown in Figure 1-1. The band lower than 10GHz has been used wildly for mobiles or other commercial purposes, such as Wi-Fi and WiMAX. That results in overcrowding and

inadequate use of this band. In the 20-40GHz, only the narrow band of microwave signal can be used and it is also insufficient to provide high-speed data transmission. However, there are several broad band above 50GHz (57-66GHz, 71-76GHz and 92-94GHz).

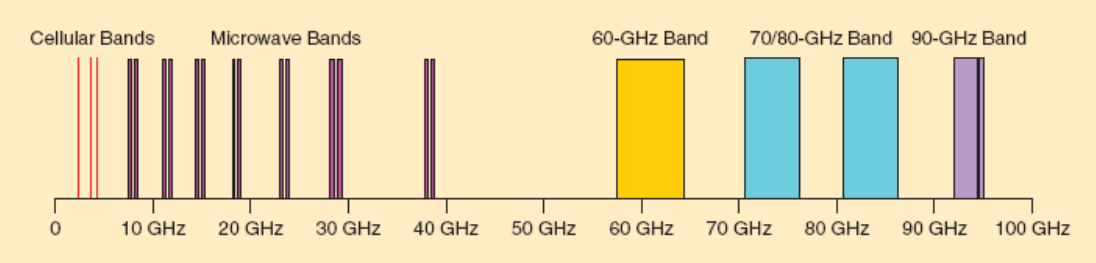


Figure 1-1 The band and the bandwidth are allowed to use in the USA.

After U.S. Federal Communications Commission opened bands with 50-120 GHz (57-64 GHz/71-76 GHz/81-86 GHz / 92-95 GHz), the industry and academia did a lot of effort to research how to develop these frequency bands [1-2]. However, based on physical characteristics, transmission distance of the high-frequency microwave radio signal is depends on different frequency, when frequency increase and transmission distance will be reduced. In order to increase the coverage of wireless signals need to use cable to transmit high-frequency microwave signal, and wireless signals will emission by antenna, but the signal loss will be a big problem when high-frequency signal use coaxial cable as a transmission medium, and high-frequency coaxial cable price is very expensive, it is not suitable for the development of high-frequency radio signal transmission. Therefore it was suggested that Radio-over- Fiber (RoF) systems to address high frequency wireless signal coverage issues.

Due to the higher frequency millimeter-wave signal has smaller coverage area. Hence, we need a lot of base stations to deliver millimeter-wave signal as

shown in Fig. 1-1. In order to saving the system cost and less equipped base stations (BSs) along with a highly centralized central station (CS) equipped with optical and mm-wave components are very importance. Using fiber transmission medium is one of the best solutions because there are wider bandwidth and much less power loss in fiber. Therefore, Radio-over-fiber (ROF) systems are attracted and more interesting for potential use in the future. Broadband wireless communications are shown in Fig. 1-2. ROF technology is a promising solution to provide multi-gigabits/sec service because of using millimeter wave band, and it has wide converge and mobility. The combination of orthogonal frequency-division multiplexing (OFDM) and radio-over-fiber (ROF) systems (OFDM-ROF) is considerable attention for future gigabit broadband wireless communication [3-7]. The high peak to average power ratio (PAPR) and nonlinear distortion of optical transmitter are the main issues raised by OFDM and ROF systems, respectively.

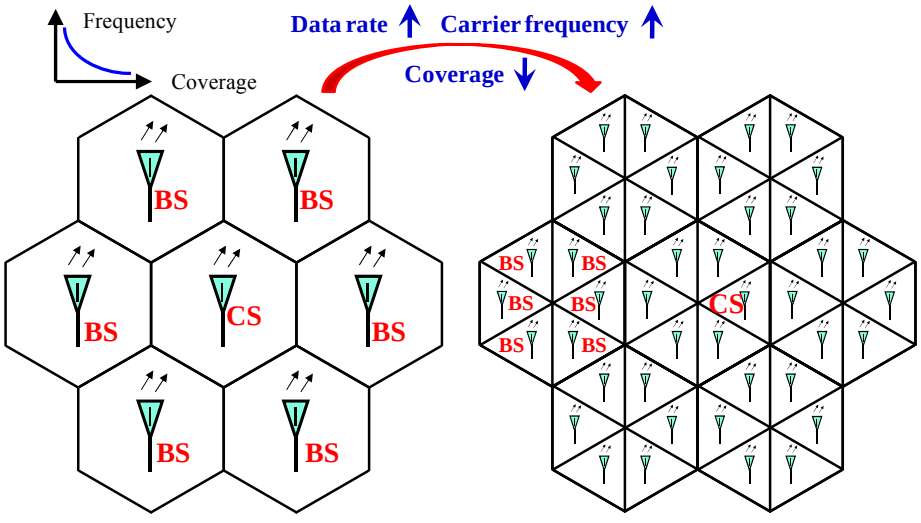


Figure 1-2 Basic structure of microwave/millimeter-wave wireless system.

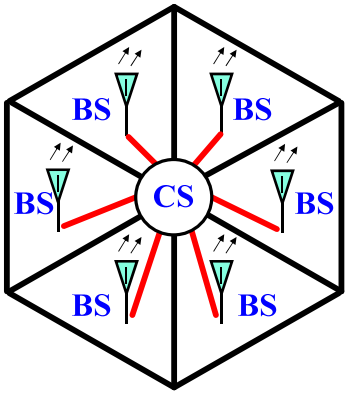


Figure 1-3 the Radio-over fiber system.

## 1.2 Motivition

In recent years, many research groups propose to use OFDM signals to solve the RoF system's problem, however, the frequency response of system is a issue, and the noise distribution is also not entirely the AWGN. The amplitude response not only affects signal energy, but also contributed to the SNR of each subcarrier good and bad. Therefore, we want to use Bit loading algorithm [8] to optimize each subcarrier's data format and power, to achieve the higher data rate.

## 1.3 Objective and Problem Statement

Rapidly increasing demand for multi-Gbps wireless communication has attacted a lot of interesting in the 7-GHz license-free spectrum at 60 GHz. Due to higher air-link loss at 60 GHz, the radio-over-fiber (RoF) system is a promising solution for extending the coverage of 60GHz wireless signals. However, 60 GHz wireless networking presents many technical challenges owing to the high carrier frequency and the wide channel bandwidth used. One

of challenges is the non-flat channel response with up to 10 dB deviation within the 7 GHz spectrum.

To overcome non-flat channel response and achieve higher data rate, orthogonal frequency division multiplexing(OFDM) system employing m-quadrature amplitude modulation (m-QAM) with high spectrum efficiency is a promising candidate. The main advantage of OFDM is that it can simultaneously transmit many subcarriers with a relatively low data rate. Therefore, each subcarrier can have a flat channel response. However, all subcarriers of the convention OFDM signal are modulated with the same data format. Thus, some subcarriers will suffer from very poor performance as the channel response have non-flat channel response, especially for 60 GHz RoF system with up to 10 dB deviation within the 7 GHz spectrum.

In order to solve different frequency response caused the signals performance was decreased, we want to use the bit-loading algorithm to optimize the signal and increase performance of system to achieve higher data rate.

# Chapter 2

# The Concept of OFDM and Bit-Loading Algorithms

## 2.1 Preface

In recent years, many research groups propose to use OFDM signals to solve the Radio-over-Fiber system's problem, however the frequency response of system is a issue, and the noise distribution is also not entirely the AWGN. The amplitude response not only affects signal energy, but also contributed to the SNR of each subcarrier good or bad. Therefore, we want to use Bit loading algorithm to optimize each subcarrier's modulation format and power to achieve the higher data rate.

## 2.2 The OFDM

### 2.2.1 The basic structure of OFDM

Orthogonal frequency division multiplexing (OFDM) [9] uses several frequencies to increase transmission capacity instead of increasing data rate of single carrier signal. Traditionally, if we want to create several different frequencies, we need several local oscillators. Adding too many oscillators would make the system complex. And OFDM system uses fast Fourier transform (FFT) and inverse fast Fourier transform (IFFT) to simplify the structure.

The transmission concept of OFDM system is shown in Fig. 2-2. At the transmitter, it maps serial data into parallel subcarriers, and then executes IFFT to get serial digital data. After DSP modulation, it uses a digital-to-analog converter to convert the digital signal to analog signal. At the receiver, it uses an analog-to-digital converter to convert analog signal to digital signal, then executes synchronization and FFT. After FFT, it equalizes data in frequency domain.

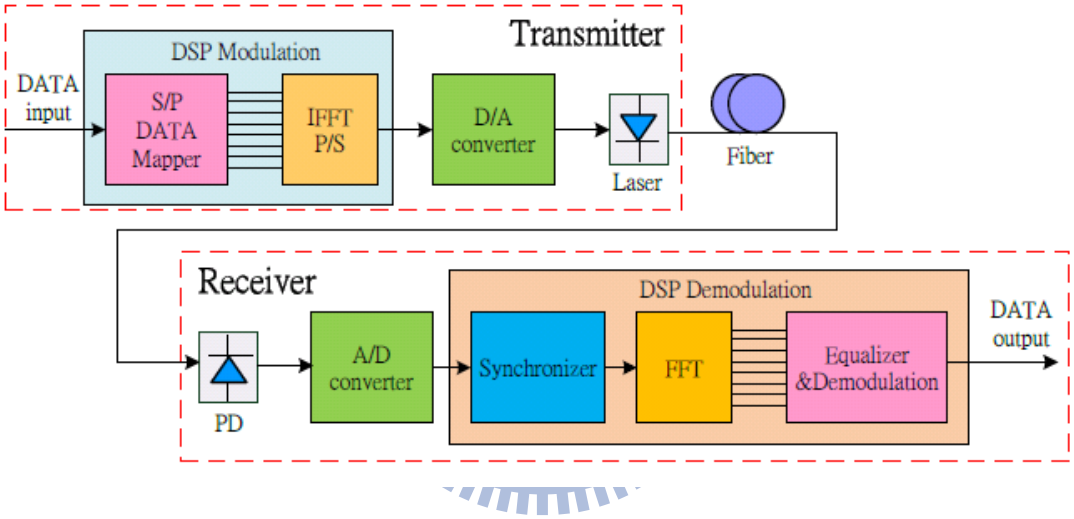


Figure 2-1 Transmission concept of OFDM system.

The OFDM has a lot of advantages such as simple equalizer, which can support high order QAM modulation for OFDM signal is strong against channel response. In addition, the orthogonal characteristic of OFDM signal can make transmission more efficient, because we can adjust the modulation type of each sub-channel according to channel response. For example, if sub-channel is located at the good channel response part, we can use high order QAM modulation format (ex: 128QAM, 64QAM) [10]. On the other hand, if sub-channel is located at the bad channel response part, we can use lower order

modulation format (ex: QPSK, BPSK). So the transmission would not be limited by the channel response.

Orthogonal frequency division multiplexing signal is composed of many narrow band subcarriers, and each subcarrier is independent. It uses multiple subcarriers to transmit low speed data instead of using signal carrier to transmit high speed data is shown in Fig. 2-3.

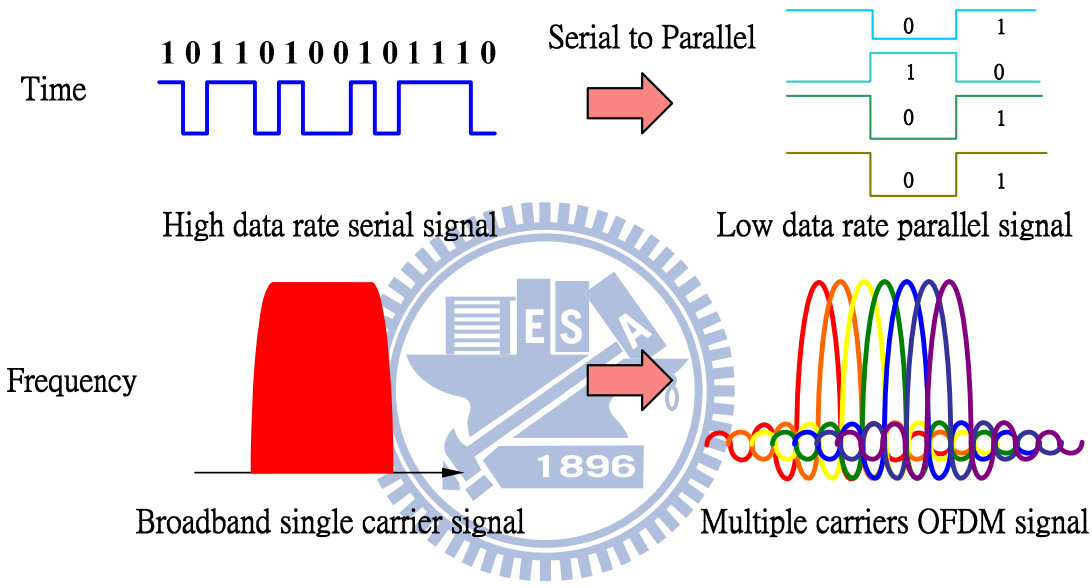


Figure 2-2 Using OFDM signal instead of broadband single carrier signal.

### 2.2.2 Advantages of using OFDM signal over fiber

**Robust against channel imperfection**

Because of the demand of high speed transmission, broadband transmission is needed. Using broadband single carrier signal to transmission data will encounter some problems. If channel response is not smooth or the components has frequency ripple in the signal's band, the signal would have

serious distortion after transmission. OFDM can solve the problem. OFDM signal uses a lot of narrow band subcarriers to transmit data (Figure. 7), so it can view the channel response of each subcarrier as flat. In addition, it can use a simple frequency domain equalizer to compensate the response of each subcarrier, so OFDM signal is robust against channel imperfection.

**Eliminates ISI through use of a cyclic prefix**

When light transmission in the fiber, it will encounter optical dispersion issue. Optical dispersion is a phenomenon that different frequency of light transmitting in the same fiber will have different transmitted speed, so a broadband signal will encounter inter symbol interference (ISI). In some conditions, i.e. single side band transmission, OFDM signal can eliminate it. In wireless communication, one of the most important characteristics of OFDM signal is that it can solve the multiple paths problem by adding cyclic prefix. We can view different frequency as different paths, so the dispersion issue is as same as multiple path issue, and OFDM signal can eliminate the ISI.

**Supporting broadband data and wireless signal simultaneously**

wireless transmission plays an important role in access network today, but its coverage is limited when we need to transmit broadband data. So we need the radio over fiber (ROF) technology to extend the coverage. Wireless signal is a narrow band signal, so we want to transmit wireless and wireline signal simultaneously. OFDM is a good choice for combining these two signals. The subcarriers of OFDM are independent and able to operate separately, so we can

turn off some subcarriers. Those vacant frequency space can provide wireless for transmission.

### 2.2.3 Disadvantages of OFDM signal

**Synchronization issues**

The OFDM signal requires precise symbol synchronization as well as frequency synchronization. OFDM signal needs precise symbol synchronization, if the symbol synchronization is not precise enough, it may induce serious inter symbol interference (ISI) especially when the sampling offset is over the cyclic prefix. And frequency synchronization includes sampling frequency synchronization and carrier frequency synchronization. OFDM signal is sensitive to frequency offset, so both sampling frequency offset and carrier frequency offset may induce ISI or destroy the orthogonality of OFDM signal.

**High peak to average power ratio**

OFDM signal is a multi-carriers signal, so its signal is the linear summation of each subcarrier, and it makes the peak to average power ratio (PAPR) of OFDM signal high. High PAPR makes the system need high linear power amplifier which increases the cost of the system. High PAPR also increases the quantization error of analog to digital (A/D) or digital to analog conversion (D/A).

## 2.3 The bit-loading algorithms

### 2.3.1 Introduction of bit-loading algorithms

The equivalent channel when transmission is carried out over SMF fiber with direct modulation remains stable in time. Large performance enhancement can, therefore, be reached in this scenario when the transceiver is designed to take into account the channel properties.OFDM modulation [11] known as discrete multitone (DMT) in wireless system is well suited to adapt the modulation order or equivalently the number of bits as well as the power level depending on the channel state information (CSI) for each subcarrier. The CSI can consist of signal-to-noise ratio (SNR) per subcarrier that can be measured at the receiver side using probing signals. As a result, subcarriers with a high SNR will be assigned more bits to transmit than subcarriers with a lower SNR. However, the same quality in terms of BER will be targeted.

Since the 60-GHz components have uneven frequency response looks like Fig. 2-4, the OFDM signal performance is limited by the subcarrier with the poorest error performance. The adaptive power and bit allocation for each subcarrier is a good solution to improve the data throughput and keep the same signal performance. Before introduce the principle of bit-loading algorithm we need to describe what is the SNR gap and the water-filling solution.

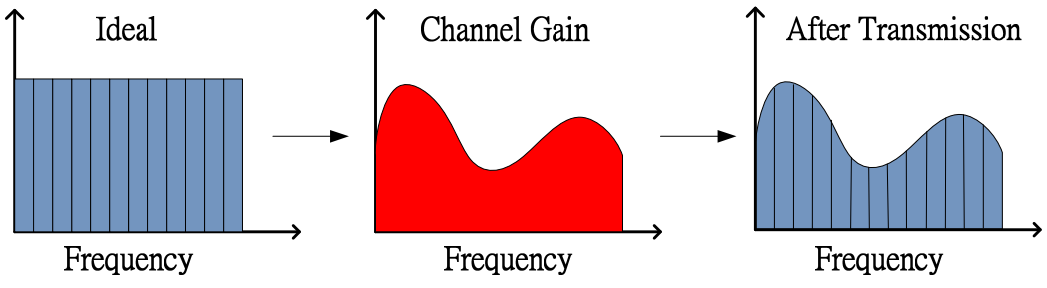


Figure 2-3 Basic concept of adaptive multi-channel transmission.

### 2.3.2 Definition of SNR gap

OFDM divides the available bandwidth into a set of N orthogonal sub-channels. With the insertion of a sufficiently long cyclic prefix, these N sub-channels can be treated as independent parallel locally-flat channels corrupted by AWGN. The SNR gap is a useful concept because it is roughly independent of the constellation size for square QAM, and is easily computable as a function of the probability of error target [12-14]. The SNR gap is used to measure the reduction of SNR with respect to capacity and it only depends on the error probability requirements.

Before introduce the bit-loading algorithm, we need to know what is the SNR gap. For $\mathrm{M}\times\mathrm{M}$-QAM, the probability of error per two dimensions is given by

$$P_s(E) \approx 4Q(\frac{\alpha}{\sigma}) \qquad \text{(Eq. 2-1)}$$

Substituting the average energy $E_s = 2\alpha^2 \frac{(M^2-1)}{3}$ per two dimensions, the noise variance $\sigma^2 = \frac{N_0}{2}$, and the normalized signal-to-noise ratio

$$SNR_{norm} = \frac{SNR}{2^\rho - 1} = \frac{E_s/N_0}{M^2-1} \qquad \text{(Eq. 2-2)}$$

We find that the factors of $M^2-1$ cancel and we obtain the performance curve

$$P_s(E) \approx 4Q(\sqrt{3SNR_{norm}}) \qquad \text{(Eq. 2-3)}$$

The curve (Eq. 2-3) of $P_s(E)$ vs. $SNR_{norm}$ for uncoded $M\times M$-QAM is plotted in Fig. 2-5, also gives us another universal design tool. For example, if we want to achieve $P_s(E)\approx 10^{-5}$ with uncoded 16-QAM (or 16-PAM), then we

know that we will need to achieve $SNR \approx 8.4dB$, the (Notice that $SNR_{norm}$, unlike $\frac{E_b}{N_0}$, is already normalized for spectral efficiency.)

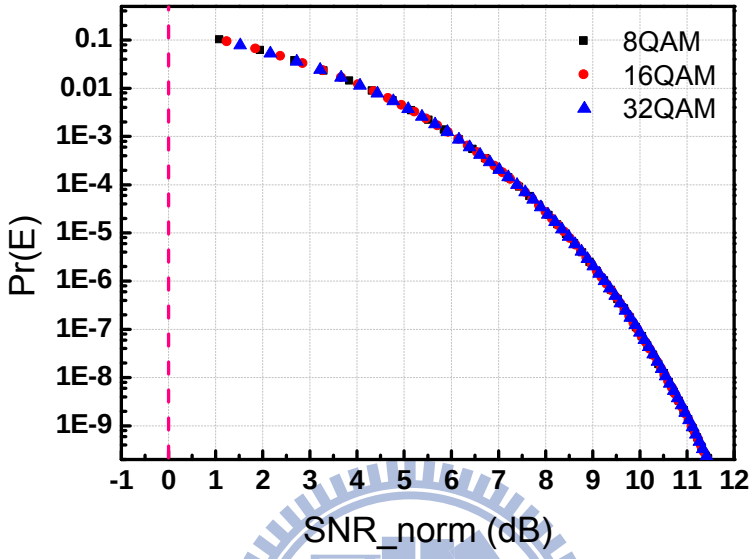


Figure 2-4 $P_s(E)$ *vs.* $SNR_{norm}$ *for nocoded* $(M \times M) - QAM$

The Shannon limit on $SNR_{norm}$ for any spectral efficiency is $SNR_{norm} > 1$ ( $o$ $dB$) .

### 2.3.3 Principle of water filling

Basically the water filling solution is according to information which is based on each channel to the bit allocation for the number of bit (modulation format), if subcarriers with high SNR will be assigned more bits and allocate power to transmit than subcarriers with a lower SNR or even turn off this subcarrier in order to avoid affecting other channel.

To maximize the data rate, for a set of parallel subchannels when the

symbol rate is fixed requires maximization of the achievable $b = \sum_n b_n$ over $b_n$ and $\varepsilon_n$. The largest number of bits that can be transmitted over a parallel set of subchannels must maximize the sum

$$b = \frac{1}{2}\sum_{n=1}^{N} \log_2\left(1 + \frac{\varepsilon_n \cdot g_n}{\Gamma}\right) \qquad \text{(Eq. 2-4)}$$

where $g_n$ represents the subchannel signal-to-noise ratio when the transmitter applies unit energy to that subchannel. $g_n$ is a fixed function of the channel, but $\varepsilon_n$ can be varied to maximize b, subject to an energy constraint that

$$\sum_{n=1}^{N} N \cdot \bar{\varepsilon}_x \qquad \text{(Eq. 2-5)}$$

Using Lagrange multipliers, the cost function to maximize (Eq. 2-4) subject to the constraint in (Eq. 2-5) becomes

$$\frac{1}{2\ln 2}\sum_n \ln\left(1 + \frac{\varepsilon_n \cdot g_n}{\Gamma}\right) + \lambda\left(\sum_n \varepsilon_n - N \cdot \bar{\varepsilon}_x\right) \qquad \text{(Eq. 2-6)}$$

Differentiating with respect to $\varepsilon_n$ produces

$$\frac{1}{2\ln 2} \cdot \frac{1}{(\Gamma / g_n) + \varepsilon_n} = -\lambda \qquad \text{(Eq. 2-7)}$$

Thus, (Eq. 2-4) is maximized, subject to (Eq. 2-5), when

$$\varepsilon_n + \frac{\Gamma}{g_n} = constant \qquad \text{(Eq. 2-8)}$$

When $\Gamma = 1$ (0 dB), the maximum data rate or capacity of the parallel set of channels is achieved. The solution is called the **water-filling solution** because one can construe the solution graphically by thinking of the curve of inverted channel signal-to-noise ratios as being filled with energy (water) to a constant line as in Fig 2-6. When $\Gamma \neq 1$, the form of the water-fill optimization remains the same (as long as $\Gamma$ is constant over all subchannels). The scaling by $\Gamma$

makes the inverse channel SNR curve, $\frac{\Gamma}{g_n}$ vs. n, appear more steep with n, thus leading to a more narrow (fewer used subchannels) optimized transmit band than when capacity ($\Gamma = 1$) is achieved. The number of bits on each subchannel is then

$$b_n = 0.5\log_2(1+\frac{\varepsilon_n \cdot g_b}{\Gamma}) \qquad \text{(Eq. 2-9)}$$

For the example of multi-tone, the optimum water-filling transmit energies then satisfy

$$\varepsilon_n + \frac{\Gamma}{g_n} = constant \qquad \text{(Eq. 2-10)}$$

Figure 2-5 depicts water-filling for a transmission system with 7 subchannels with $g_n$. Equation (Eq. 2-10) is solved for the constant when $\sum_n \varepsilon_n = N \cdot \bar{\varepsilon}_x$ and $\bar{\varepsilon}_x \geq 0$. Four of the six subchannels in Fig. 2-6 have positive energies, while one were eliminated for having negative energy, or equivalently having a noise power that exceeded the constant **water line** of water filling. The 6 used subchannels have energy that makes the sum of normalized noise and transmit energy constant. For methods of computing the water-fill solution, see the next section. The term energy collinge, power also smaller, and sometimes of $\frac{\Gamma}{g_n}$ being a bowl into which water (energy) is poured, filling the bowl until there is no more energy to use. The water will rise to a constant flat level in the bowl. The amount of water/energy in any subchannel is the depth of the water at the corresponding point in the bowl.

The water-filling solution is unique because the function being minimized is convex, so there is a unique optimum energy distribution (and corresponding set of subchannel data rates) for each ISI channel with multi-channel modulation.

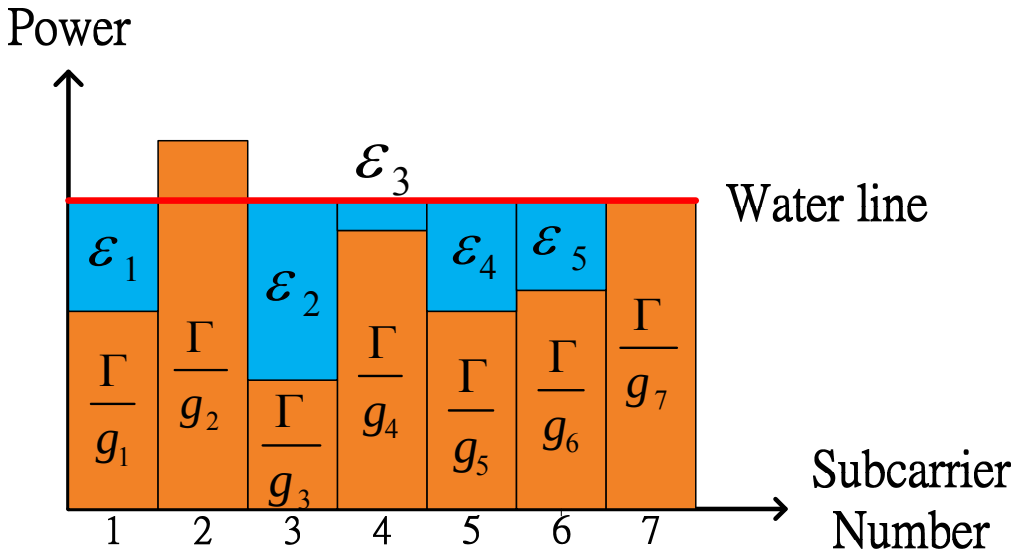


Figure 2-5 Illustration of discrete water-filling of 7 subchannels.

### 2.3.4 Principle of bit-loading algorithms

There are two types of bit-loading algorithms – those that try to maximize data rate(Rate-Adaptive (RA) loading criterion) and those that try to maximize performance at a given fixed data rate (Margin-Adaptive (MA) loading criterion). In this research we chose the RA loading to optimize each subcarriers. A rate-adaptive loading procedure maximizes (or approximately maximizes) the number of bits per symbol subject to a fixed energy constraint:

$$b_{\max} = \sum_{n=1}^{N} \frac{1}{2} \log_2 \left(1 + \frac{\varepsilon_n \cdot g_n}{\Gamma}\right) \qquad \text{(Eq. 2-11)}$$

$$\text{Subject to: } g = \sum_{n=1}^{N} \varepsilon_n \qquad \text{(Eq. 2-12)}$$

The set of linear equations that has the water-fill distribution as its solution is

$$\begin{aligned}
\varepsilon_1 + \frac{\Gamma}{g_1} &= k \\
\varepsilon_2 + \frac{\Gamma}{g_2} &= k \\
&\vdots \\
\varepsilon_N + \frac{\Gamma}{g_N} &= k \\
\varepsilon_1 + \varepsilon_2 \cdots + \varepsilon_N &= g
\end{aligned} \qquad \text{(Eq. 2-13)}$$

There are a maximum of N + 1 equations in N + 1 unknowns. The unknowns are the energies $\varepsilon_n$, $n = 1, 2 \ldots N$ and the constant K. The solution can produce negative energies. If it does, the equation with the smallest $g_n$ should be eliminated, and the corresponding $\varepsilon_n$ should be zeroed. The remaining sets of equations are solved recursively by eliminating the smallest $g_n$ and zeroing $\varepsilon_n$, until the first solution with no negative energies occurs. In matrix form, the equations become

$$\begin{bmatrix} 1 & 0 & 0 & \cdots & -1 \\ 0 & 1 & 0 & \cdots & -1 \\ \vdots & \vdots & \vdots & \ddots & -1 \\ 1 & 1 & 1 & \cdots & 1 \; 0 \end{bmatrix} \begin{bmatrix} \varepsilon_1 \\ \varepsilon_1 \\ \vdots \\ \varepsilon_N \\ k \end{bmatrix} = \begin{bmatrix} -\Gamma/g_1 \\ -\Gamma/g_2 \\ \vdots \\ -\Gamma/g_N \\ g \end{bmatrix} \qquad \text{(Eq. 2-14)}$$

which are readily solved by matrix inversion. Matrix inversions of size N +1 down to 1 may have to be performed iteratively until nonnegative energies are found for all subchannels. An alternative solution sums the first N equations to obtain:

$$k = \frac{1}{N}\left[ g + \Gamma \cdot \sum_{n=1}^{N} \frac{1}{g_n} \right] \qquad \text{(Eq. 2-15)}$$

If one or more of $\varepsilon_n < 0$, then the most negative is eliminated, and (Eq.

2-15) is solved again with N → N − 1 and the corresponding $g_n$ term eliminated. The equations preferably are preordered in terms of signal-to-noise ratio with n = 1 corresponding to the largest-SNR subchannel $g_1 = \max_n g_n$ and n = N corresponding to the smallest-SNR subchannel $g_N = \min_n g_n$. Equation (4.42) then becomes at the $i^{th}$ step of the iteration (i = 0, …N)

$$k = \frac{1}{N-i}\left[\varepsilon + \Gamma \cdot \sum_{n=1}^{N-i} \frac{1}{g_n}\right] \qquad \text{(Eq. 2-16)}$$

The water-filling algorithm is illustrated by the flow chart of Figure 4.7. The sum in the expression for K in (4.42) is always over the used subchannels. The following simplified formulae, apparently first observed by Aslanis, then determine the number of bits and number of bits per dimension as

$$b_n = \frac{1}{2}\log_2\left(\frac{K \cdot g_n}{\Gamma}\right) = \frac{1}{2}\log_2\left(1 + \frac{\varepsilon_n \cdot g_n}{\Gamma}\right) \qquad \text{(Eq. 2-17)}$$

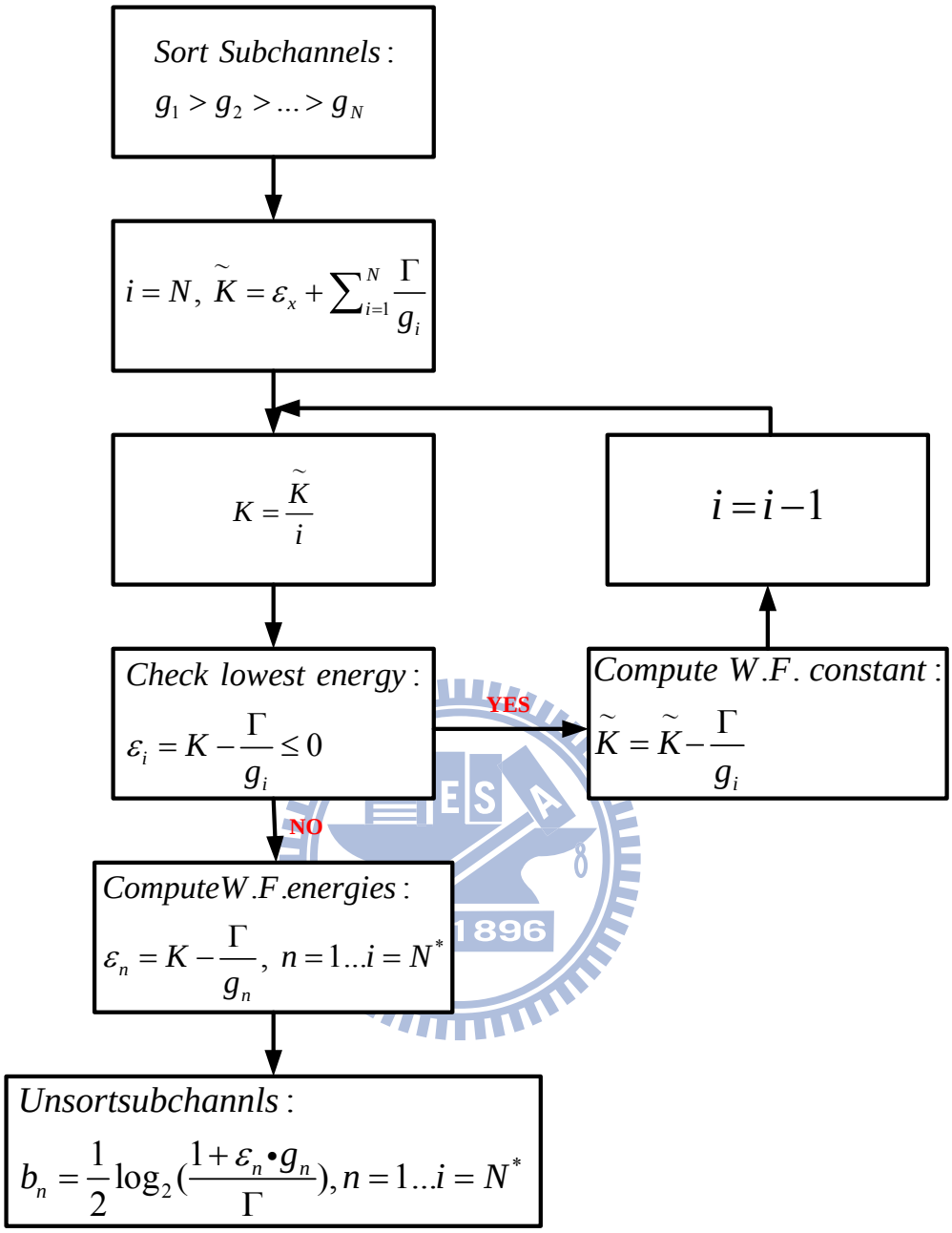


Figure 2-6 Flow chart of Rate-Adaptive water-filling algorithm.

# Chapter 3

## The theoretical calculations of proposed system

### 3.1 Introduce MZM

For MZM with configuration as Fig. 3-1, the output E-filed for upper arm is

$$E_U = E_0 \cdot a \cdot e^{j\Delta\varphi_1} \quad \text{(Eq. 3-1)}$$

$$\Delta\varphi_1 \triangleq \frac{V_1}{V_\pi} \cdot \pi \quad \text{(Eq. 3-2)}$$

$\Delta\varphi_1$ is the optical carrier phase difference that is induced by $V_1$, where a is the power splitting ratio.

The output E-filed for upper arm is

$$E_L = E_0 \cdot \sqrt{1-a^2} \cdot e^{j\Delta\varphi_2} \quad \text{(Eq. 3-3)}$$

$\Delta\varphi_2$ is the optical carrier phase difference that is induced by $V_2$

$$\Delta\varphi_2 \triangleq \frac{V_2}{V_\pi} \cdot \pi \quad \text{(Eq. 3-4)}$$

The output E-filed for MZM is

$$E_T = E_0 \cdot \{a \cdot b \cdot e^{j\Delta\varphi_1} + \sqrt{1-a^2} \cdot \sqrt{1-b^2} \cdot e^{j\Delta\varphi_2}\} \quad \text{(Eq. 3-5)}$$

where a and b are the power splitting ratios of the first and second Y-splitters in MZM, respectively. The power splitting ratio of two arms of a balanced MZM is 0.5. The electrical field at the output of the MZM is given by

$$E_T = \frac{1}{2} \cdot E_0 \cdot \{e^{j\Delta\varphi_1} + e^{j\Delta\varphi_2}\} \quad \text{(Eq. 3-6)}$$

$$E_T = E_0 \cdot \cos(\frac{\Delta\varphi_1 - \Delta\varphi_2}{2}) \cdot \exp(j \cdot \frac{\Delta\varphi_1 + \Delta\varphi_2}{2}) \quad \text{(Eq. 3-7)}$$

For single electro x-cut MZM, the electrical field at the output is given by

$$E_{out} = E_0 \cdot \cos(\frac{\Delta\varphi - (-\Delta\varphi)}{2}) \cdot \exp(j \cdot \frac{\Delta\varphi + (-\Delta\varphi)}{2}) \quad \text{(Eq. 3-8)}$$

Add time component, the electrical field is

$$E_{out} = E_0 \cdot \cos(\Delta\varphi) \cdot \cos(\omega_0 t) \quad \text{(Eq. 3-9)}$$

where $E_0$ and $\omega_c$ denote the amplitude and angular frequency of the input optical carrier, respectively; $V(t)$ is the applied driving voltage, and $\Delta\varphi$ is the optical carrier phase difference that is induced by $V(t)$ between the two arms of the MZM. The loss of MZM is neglected. $V(t)$ consisting of an electrical sinusoidal signal and a dc biased voltage can be written as

$$V(t) = V_{bias} + V_m \cos(\omega t) \quad \text{(Eq. 3-10)}$$

where $V_{bias}$ is the dc biased voltage, $V_m$ and $\omega_{RF}$ are the amplitude and the angular frequency of the electrical driving signal, respectively. The optical carrier phase difference induced by $V(t)$ is given by

$$\Delta\varphi = \frac{V(t)}{2V_\pi} = \frac{V_{bias} + V_m \cdot \cos(\omega t)}{V_\pi} \cdot \frac{\pi}{2} \quad \text{(Eq. 3-11)}$$

Eq. 3-10 can be written as

$$\begin{aligned} E_{out} &= E_0 \cdot \cos[\frac{V_{bias} + V_m \cdot \cos(\omega t)}{V_\pi} \cdot \frac{\pi}{2}] \cdot \cos(\omega_0 t) \\ &= E_0 \cdot \cos[b + m \cdot \cos(\omega_{RF} t)] \cdot \cos(\omega_0 t) \\ &= E_0 \cdot \cos(\omega_0 t) \cdot \{\cos(b) \cdot \cos[m \cdot \cos(\omega_{RF} t)] \\ &\quad - \sin(b) \sin[m \cdot \cos(\omega_{RF} t)]\} \end{aligned} \quad \text{(Eq. 3-12)}$$

where $b \triangleq \frac{V_{bias}}{2V_\pi} \cdot \pi$ is a constant phase shift that is induced by the DC biased voltage, and $m \triangleq \frac{V_m}{2V_\pi \cdot \pi}$ is the phase modulation index.

$$\begin{cases} \cos(x \cdot \sin(\theta)) = J_0(x) + 2\sum_{n=1}^{\infty} J_{2n}(x) \cdot \cos(2n\theta) \\ \sin(x \cdot \sin(\theta)) = 2\sum_{n=1}^{\infty} J_{2n-1}(x) \cdot \sin[(2n-1)\theta] \end{cases} \quad \text{(Eq. 3-13)}$$

$$\begin{cases} \cos(x \cdot \cos(\theta)) = J_0(x) + 2\sum_{n=1}^{\infty} (-1)^n J_{2n}(x) \cdot \cos(2n\theta) \\ \sin(x \cdot \cos(\theta)) = 2\sum_{n=1}^{\infty} (-1)^n J_{2n-1}(x) \cdot \cos[(2n-1)\theta] \end{cases} \quad \text{(Eq. 3-14)}$$

Expanding Eq. 3-12 using Bessel functions, as detailed in Eq. 3-13. The electrical field at the output of the MZM can be written as

$$\begin{aligned} E_{out} = E_0 \cdot \cos(\omega_0 t) \cdot & \\ \{\cos(b) \cdot [J_0(m) + 2\sum_{i=1}^{\infty} (-1)^n \cdot J_{2n}(m) \cdot \cos(2n\omega_{RF} t)] & \quad \text{(Eq. 3-15)} \\ -\sin(b) \cdot [2\sum_{i=1}^{\infty} (-1)^n \cdot J_{2n-1}(m) \cdot \cos[(2n-1)\omega_{RF} t]]\} & \end{aligned}$$

where $J_n$ is the Bessel function of the first kind of order n. the electrical field of the mm-wave signal can be written as

$$\begin{aligned} E_{out} &= E_0 \cdot \cos(b) \cdot J_0(m) \cdot \cos(\omega_0 t) \\ &+ E_0 \cdot \cos(b) \cdot \sum_{i=1}^{\infty} J_{2n}(m) \cdot \cos[(\omega_0 - 2n\omega_{RF})t + n\pi] \\ &+ E_0 \cdot \cos(b) \cdot \sum_{i=1}^{\infty} J_{2n}(m) \cdot \cos[(\omega_0 + 2n\omega_{RF})t + n\pi] \quad \text{(Eq. 3-16)} \\ &- E_0 \cdot \sin(b) \cdot \sum_{i=1}^{\infty} J_{2n-1}(m) \cdot \cos[(\omega_0 - (2n-1)\omega_{RF})t + n\pi] \\ &- E_0 \cdot \sin(b) \cdot \sum_{i=1}^{\infty} J_{2n-1}(m) \cdot \cos[(\omega_0 + (2n-1)\omega_{RF})t + n\pi] \end{aligned}$$

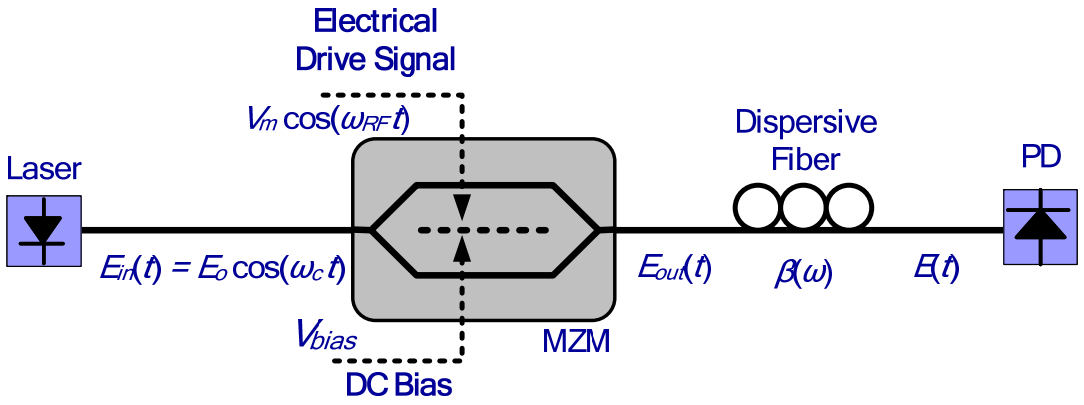


Figure 3-1 The principle diagram of the optical mm-wave generation using balanced MZM.

## 3.2 Theoretical calculation of single drive MZM

### 3.2.1 Bias at maximum transmission point

When the MZM is biased at the maximum transmission point, the bias voltage is set at $V_{bias} = 0$, and $\cos(b) = 1$ and $\sin(b) = 0$. Consequently, the electrical field of the mm-wave signal can be written as

$$\begin{aligned} E_{out} &= E_0 \cdot J_0(m) \cdot \cos(\omega_0 t) \\ &+ E_0 \cdot \sum_{i=1}^{\infty} J_{2n}(m) \cdot \cos[(\omega_0 - 2n\omega_{RF})t + n\pi] \\ &+ E_0 \cdot \sum_{i=1}^{\infty} J_{2n}(m) \cdot \cos[(\omega_0 + 2n\omega_{RF})t + n\pi] \end{aligned} \qquad \text{(Eq. 3-17)}$$

The amplitudes of the generated optical sidebands are proportional to those of the corresponding Bessel functions associated with the phase modulation index $m$. With the amplitude of the electrical driving signal $V_m$ equal to $V_\pi$, the maximum $m$ is $\frac{\pi}{2}$. As $0 < m < \frac{\pi}{2}$, the Bessel function $J_n$ for $n \geq 1$ decreases and increases with the order of Bessel function and m,

respectively, as shown in Figure 3-2. $J_1(\frac{\pi}{2})$, $J_2(\frac{\pi}{2})$, $J_3(\frac{\pi}{2})$, and $J_4(\frac{\pi}{2})$ are 0.5668, 0.2497, 0.069, and 0.014, respectively. Therefore, the optical sidebands with the Bessel function higher than $J_3(m)$ can be ignored, and Eq. 3-15 can be further simplified to

$$\begin{aligned} E_{out} &= E_0 \cdot J_0(m) \cdot \cos(\omega_0 t) \\ &+ E_0 \cdot J_2(m) \cdot \cos[(\omega_0 - 2\omega_{RF})t + \pi] \\ &+ E_0 \cdot J_2(m) \cdot \cos[(\omega_0 + 2\omega_{RF})t + \pi] \\ &+ E_0 \cdot J_4(m) \cdot \cos[(\omega_0 - 4\omega_{RF})t] \\ &+ E_0 \cdot J_4(m) \cdot \cos[(\omega_0 + 4\omega_{RF})t] \end{aligned} \qquad \text{(Eq. 3-18)}$$

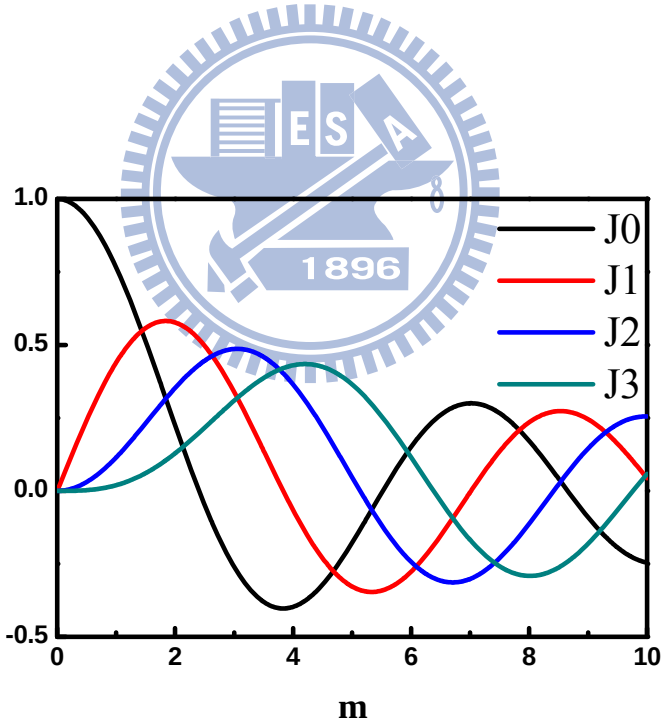


Figure 3-2 The different order of Bessel functions vs. m.

### 3.2.2 Bias at quadrature point

When the MZM is biased at the quadrature point, the bias voltage is set at $V_{bias} = \frac{V_\pi}{2}$, and $\cos(b) = \frac{\sqrt{2}}{2}$ and $\sin(b) = \frac{\sqrt{2}}{2}$. Consequently, the electrical field of the mm-wave signal can be written as

$$\begin{aligned} E_{out} = & \frac{1}{\sqrt{2}} E_0 \cdot J_0(m) \cdot \cos(\omega_0 t) \\ & + \frac{1}{\sqrt{2}} E_0 \cdot J_1(m) \cdot \cos[(\omega_0 - \omega_{RF})t] \\ & + \frac{1}{\sqrt{2}} E_0 \cdot J_1(m) \cdot \cos[(\omega_0 + \omega_{RF})t] \\ & + \frac{1}{\sqrt{2}} E_0 \cdot J_2(m) \cdot \cos[(\omega_0 - 2\omega_{RF})t + \pi] \\ & + \frac{1}{\sqrt{2}} E_0 \cdot J_2(m) \cdot \cos[(\omega_0 + 2\omega_{RF})t + \pi] \\ & + \frac{1}{\sqrt{2}} E_0 \cdot J_3(m) \cdot \cos[(\omega_0 - 3\omega_{RF})t + \pi] \\ & + \frac{1}{\sqrt{2}} E_0 \cdot J_3(m) \cdot \cos[(\omega_0 + 3\omega_{RF})t + \pi] \end{aligned} \qquad \text{(Eq. 3-19)}$$

### 3.2.3 Bias at null point

When the MZM is biased at the null point, the bias voltage is set at $V_{bias} = V_\pi$, and $\cos(b) = 0$ and $\sin(b) = 1$. Consequently, the electrical field of the mm-wave signal using DSBCS modulation can be written as

$$
\begin{aligned}
E_{out} &= E_0 \cdot J_1(m) \cdot \cos[(\omega_0 - \omega_{RF})t) \\
&+ E_0 \cdot J_1(m) \cdot \cos[(\omega_0 + \omega_{RF})t] \\
&+ E_0 \cdot J_3(m) \cdot \cos[(\omega_0 - 3\omega_{RF})t + \pi] \\
&+ E_0 \cdot J_3(m) \cdot \cos[(\omega_0 + 3\omega_{RF})t + \pi] \\
&+ E_0 \cdot J_5(m) \cdot \cos[(\omega_0 - 5\omega_{RF})t] \\
&+ E_0 \cdot J_5(m) \cdot \cos[(\omega_0 + 5\omega_{RF})t]
\end{aligned}
\qquad \text{(Eq. 3-20)}
$$

## 3.3 Theoretical calculations and simulation results

### 3.3.1 The generated optical signal

The theoretical calculations of proposed system, the driving RF signal $V(t)$ consisting of an electrical sinusoidal signal and a dc biased voltage can be written as

$$V(t) = V_{bias} + V_1 \cos(\omega_1 t) + V_2 \cos(\omega_2 t) \qquad \text{(Eq. 3-21)}$$

where $V_{bias}$ is the dc biased voltage, $V_1$, $V_2$ and $\omega_1$, $\omega_2$ are the amplitude and the angular frequency of the electrical driving signals, respectively. The optical carrier phase difference induced by $V(t)$ is given by

$$
\begin{aligned}
E_{out} &= E_0 \cdot \cos[\frac{\pi}{2V_\pi}(V_{bias} + V_1 \cos(\omega_1 t) + V_2 \cos(\omega_2 t))] \\
&= E_0 \cdot \cos[b + m_1 \cos(\omega_1 t) + m_2 \cos(\omega_2 t))]
\end{aligned}
\qquad \text{(Eq. 3-22)}
$$

where $b \triangleq \frac{V_{bias} \cdot \pi}{2\pi}$ is a constant phase shift that is induced by the DC biased voltage, and $m_1 = \frac{V_1 \cdot \pi}{2V_\pi}$, $m_2 = \frac{V_2 \cdot \pi}{2V_\pi}$ is the phase modulation index.

$$
\begin{aligned}
E_{out} &= E_0 \cdot \cos(b) \cdot \cos[m_1 \cos(\omega_1 t) + m_2 \cos(\omega_2 t)] \\
&\quad - E_0 \cdot \sin(b) \cdot \sin[m_1 \cos(\omega_1 t) + m_2 \cos(\omega_2 t)] \\
&= E_0 \cdot \cos(b) \cdot \{\cos[m_1 \cos(\omega_1 t)] \cdot \cos[m_2 \cos(\omega_2 t)] \\
&\quad - \sin[m_1 \cos(\omega_1 t)] \cdot \sin[m_2 \cos(\omega_2 t)]\} \\
&\quad - E_0 \cdot \sin(b) \cdot \{\sin[m_1 \cos(\omega_1 t)] \cdot \cos[m_2 \cos(\omega_2 t)] \\
&\quad + \cos[m_1 \cos(\omega_1 t)] \cdot \sin[m_2 \cos(\omega_2 t)]\}
\end{aligned}
\qquad \text{(Eq. 3-23)}
$$

When the MZM is biased at the null point, the bias voltage is set at $V_{bias} = V_\pi$, and $\cos(b) = 0$ and $\sin(b) = 1$. Consequently, the electrical field of the mm-wave signal using DSBCS modulation can be written as

$$
\begin{aligned}
E_{out} &= -E_0 \cdot \{\sin[m_1 \cos(\omega_1 t)] \cdot \cos[m_2 \cos(\omega_2 t)] \\
&\quad + \cos[m_1 \cos(\omega_1 t)] \cdot \sin[m_2 \cos(\omega_2 t)]\}
\end{aligned}
\qquad \text{(Eq. 3-24)}
$$

First, to expand equation $\sin[m_1 \cos(\omega_1 t)]\cos[m_2 \cos(\omega_2 t)]$

$$
\begin{aligned}
&\sin[m_1 \cos(\omega_1 t)]\cos[m_2 \cos(\omega_2 t)] \\
&= \left\{2\sum_{n=1}^{\infty}(-1)^n J_{2n-1}(m_1)\cos[(2n-1)\omega_1 t]\right\} \\
&\quad \cdot \left\{J_0(m_2) + 2\sum_{n=1}^{\infty}(-1)^n J_{2n}(m_2)\cos(2n\omega_2 t)\right\} \\
&= \{-2J_1(m_1)\cos(\omega_1 t) + 2J_3(m_1)\cos(3\omega_1 t) - \cdots\} \\
&\quad \cdot \{J_0(m_2) - 2J_2(m_2)\cos(2\omega_2 t) + 2J_4(m_2)\cos(4\omega_2 t) - \cdots\}
\end{aligned}
\qquad \text{(Eq. 3-25)}
$$

The optical sidebands with the Bessel function higher than $J_3(m)$ can be ignored. Consequently, the electrical field can be written as

$$\sin[m_1\cos(\omega_1 t)]\cos[m_2\cos(\omega_2 t)]$$
$$\approx -2J_0(m_2)J_1(m_1)\cos(\omega_1 t)$$
$$+2J_0(m_2)J_3(m_1)\cos(3\omega_1 t) \qquad \text{(Eq. 3-26)}$$
$$+4J_1(m_1)J_2(m_2)\cdot\frac{1}{2}[\cos(\omega_1+2\omega_2)t+\cos(\omega_1-2\omega_2)t]$$
$$-4J_2(m_2)J_3(m_1)\cdot\frac{1}{2}[\cos(3\omega_1+2\omega_2)t+\cos(3\omega_1-2\omega_2)t]$$

Add time component $\cos(\omega_c t)$

$$\sin[m_1\cos(\omega_1 t)]\cos[m_2\cos(\omega_2 t)]\cos(\omega_c t)$$
$$\approx -2J_0(m_2)J_1(m_1)\cos(\omega_1 t)\cos(\omega_c t)$$
$$+2J_0(m_2)J_3(m_1)\cos(3\omega_1 t)\cos(\omega_c t) \qquad \text{(Eq. 3-27)}$$
$$+4J_1(m_1)J_2(m_2)\cdot\frac{1}{2}[\cos(\omega_1+2\omega_2)t+\cos(\omega_1-2\omega_2)t]\cos(\omega_c t)$$
$$-4J_2(m_2)J_3(m_1)\cdot\frac{1}{2}[\cos(3\omega_1+2\omega_2)t+\cos(3\omega_1-2\omega_2)t]\cos(\omega_c t)$$

$J_0(m_2)J_1(m_1)$ , $2J_0(m_2)J_3(m_1)$ , $4J_1(m_1)J_2(m_2)$ and $4J_2(m_2)J_3(m_1)$ are shown in Fig. 3-3. Therefore, the optical sidebands with the Bessel function $4J_2(m_2)J_3(m_1)$ can be ignored, and Eq. 3-14 can be further simplified to

$$\sin[m_1\cos(\omega_1 t)]\cos[m_2\cos(\omega_2 t)]\cos(\omega_c t)$$
$$=-J_0(m_2)J_1(m_1)[\cos(\omega_c+\omega_1)t+\cos(\omega_c-\omega_1)t]$$
$$+J_0(m_2)J_3(m_1)[\cos(\omega_c+3\omega_1)t+\cos(\omega_c-3\omega_1)t] \qquad \text{(Eq. 3-28)}$$
$$+J_1(m_1)J_2(m_2)[\cos(\omega_c+\omega_1+2\omega_2)t+\cos(\omega_c-\omega_1-2\omega_2)t]$$
$$+J_1(m_1)J_2(m_2)[\cos(\omega_c+\omega_1-2\omega_2)t+\cos(\omega_c-\omega_1+2\omega_2)t]$$

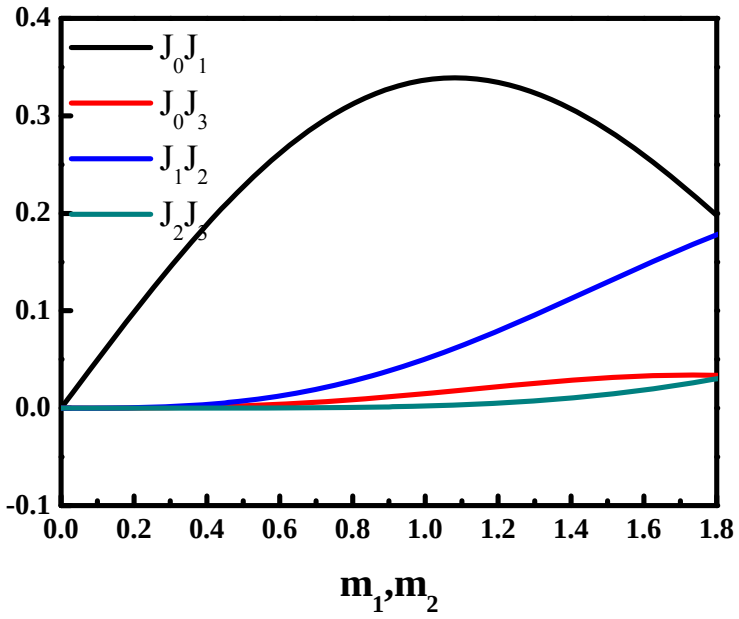


Figure 3-3 The different order of Bessel functions vs. m.

To expand equation $\cos(m_1\cos\omega_1 t)\sin(m_2\cos\omega_2 t)$

$$\cos[m_1\cos(\omega_1 t)]\sin[m_2\cos(\omega_2 t)]$$

$$= \left\{ J_0(m_1) + 2\sum_{n=1}^{\infty}(-1)^n J_{2n}(m_1)\cos(2n\omega_1 t) \right\}$$

$$\cdot \left\{ 2\sum_{n=1}^{\infty}(-1)^n J_{2n-1}(m_2)\cos[(2n-1)\omega_1 t] \right\}$$

$$= \left\{ J_0(m_1) - 2J_2(m_1)\cos(2\omega_1 t) + 2J_4(m_1)\cos(4\omega_1 t) - \cdots \right\}$$

$$\cdot \left\{ -2J_1(m_2)\cos(\omega_2 t) + 2J_3(m_2)\cos(3\omega_2 t) - \cdots \right\}$$

$$\approx -2J_0(m_1)J_1(m_2)\cos(\omega_2 t)$$

$$+ 2J_0(m_1)J_3(m_2)\cos(3\omega_2 t)$$

$$+ 4J_1(m_2)J_2(m_1)\cdot\frac{1}{2}[\cos(\omega_2 + 2\omega_1)t + \cos(\omega_2 - 2\omega_1)t]$$

$$- 4J_2(m_1)J_3(m_2)\cdot\frac{1}{2}[\cos(3\omega_2 + 2\omega_1)t + \cos(3\omega_2 - 2\omega_1)t] \qquad \text{(Eq. 3-29)}$$

Add time component $\cos(\omega_c t)$

$$\begin{aligned}
&\cos[m_1\cos(\omega_1 t)]\sin[m_2\cos(\omega_2 t)]\cos(\omega_c t)\\
&= -2J_0(m_1)J_1(m_2)\cos(\omega_2 t)\cos(\omega_c t)\\
&\quad + 2J_0(m_1)J_3(m_2)\cos(3\omega_2 t)\cos(\omega_c t)\\
&\quad + 4J_1(m_2)J_2(m_1)\cdot\frac{1}{2}[\cos(\omega_2+2\omega_1)t+\cos(\omega_2-2\omega_1)t]\cos(\omega_c t)\\
&\quad - 4J_2(m_1)J_3(m_2)\cdot\frac{1}{2}[\cos(3\omega_2+2\omega_1)t+\cos(3\omega_2-2\omega_1)t]\cos(\omega_c t)\\
&= -J_0(m_1)J_1(m_2)[\cos(\omega_c+\omega_2)t+\cos(\omega_c-\omega_2)t]\\
&\quad + J_0(m_1)J_3(m_2)[\cos(\omega_c+3\omega_2)t+\cos(\omega_c-3\omega_2)t]\\
&\quad + J_1(m_2)J_2(m_1)[\cos(\omega_c+\omega_2+2\omega_1)t+\cos(\omega_c-\omega_2-2\omega_1)t]\\
&\quad + J_1(m_2)J_2(m_1)[\cos(\omega_c+\omega_2-2\omega_1)t+\cos(\omega_c-\omega_2+2\omega_1)t]
\end{aligned} \qquad \text{(Eq. 3-30)}$$

The output electrical filed can be rewritten as

$$\begin{aligned}
E_{out}(t) = E_0\cos(\omega_c t)\{&\sin[m_1\cos(\omega_1 t)]\cos[m_2\cos(\omega_2 t)]\}\\
&+\cos[m_1\cos(\omega_1 t)]\sin[m_2\cos(\omega_2 t)]
\end{aligned} \qquad \text{(Eq. 3-31)}$$

$$\begin{aligned}
E_{out}(t) = E_0\cdot\{&J_0(m_2)J_1(m_1)[\cos(\omega_c+\omega_1)t+\cos(\omega_c-\omega_1)t]\\
&- J_0(m_2)J_3(m_1)[\cos(\omega_c+3\omega_1)t+\cos(\omega_c-3\omega_1)t]\\
&- J_1(m_1)J_2(m_2)[\cos(\omega_c+\omega_1+2\omega_2)t+\cos(\omega_c-\omega_1-2\omega_2)t]\\
&- J_1(m_1)J_2(m_2)[\cos(\omega_c+\omega_1-2\omega_2)t+\cos(\omega_c-\omega_1+2\omega_2)t]\\
&+ J_0(m_1)J_1(m_2)[\cos(\omega_c+\omega_2)t+\cos(\omega_c-\omega_2)t]\\
&- J_0(m_1)J_3(m_2)[\cos(\omega_c+3\omega_2)t+\cos(\omega_c-3\omega_2)t]\\
&- J_1(m_2)J_2(m_1)[\cos(\omega_c+\omega_2+2\omega_1)t+\cos(\omega_c-\omega_2-2\omega_1)t]\\
&- J_1(m_2)J_2(m_1)[\cos(\omega_c+\omega_2-2\omega_1)t+\cos(\omega_c-\omega_2+2\omega_1)t]\}
\end{aligned} \qquad \text{(Eq. 3-32)}$$

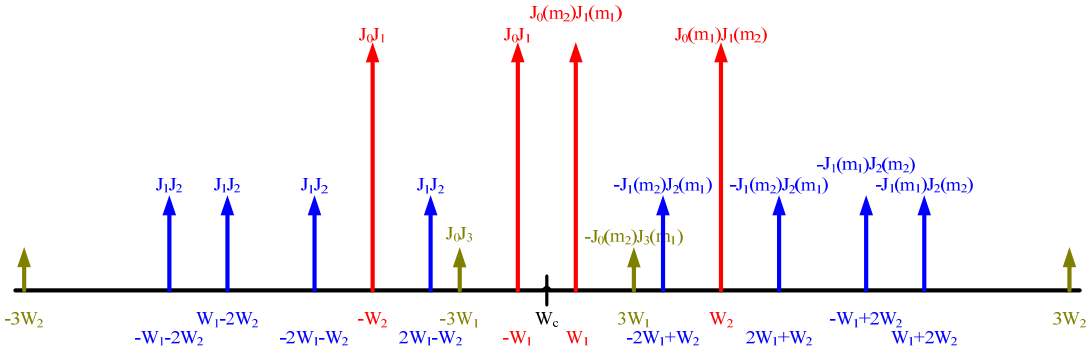


Figure 3-4 Illustration of the optical spectrum at the output of the MZM.

$(\omega_2 = 6\omega_1)$

# Chapter 4

## Experimental Demonstration of System for Wire

### 4.1 Preface

In chapter 3, we show the principle of bit-loading algorithm and we also provide the theoretical and numerical results for the concept of system. Therefore, the results can be tried to apply to the radio-over-fiber system. In this chapter, we will build the experimental setup for the system based on DSBCS modulation.

### 4.2 Experimental setup

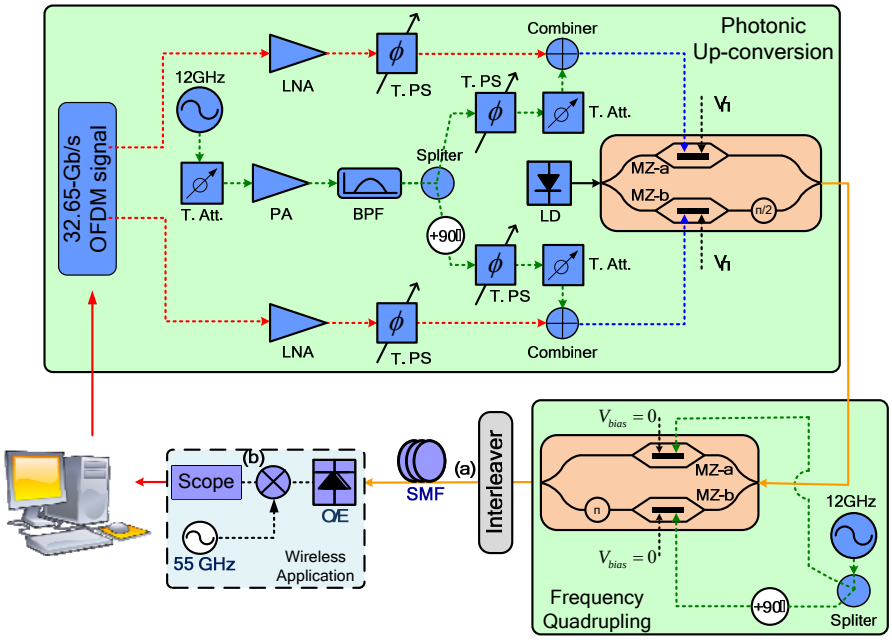


Figure 4-1 Experimental setup for all optical up-conversion.

Figure 4-1 depicts the experimental setup for all optical I/Q up conversion system via a I/Q modulator. We use a continue wave tunable laser (CW-TL) to generate light source about 1550nm. The light source is then passed through a polarization controller to achieve max optical power when the I/Q modulator is biased at full point. The signals (signal-I and signal-Q) are generated by a Tektronix ® AWG7102 arbitrary waveform generator (AWG) using a Matlab® program. The sample rate and digital-to-analog converter (DAC) resolution of the AWG are 10 Gb/s and 8 bits, respectively. And we generation four different OFDM signals, 20.625Gb/s 8-QAM OFDM signals, 27.5Gb/s 16-QAM OFDM signals and 34.375Gb/s 32-QAM OFDM signals, all of them have the same parameter, the IFFT length is 128, a 78.125MSyn/s m-QAM symbol is encoded at 88 channels (i.e. channels 2-45 and 85-128) with the remaining 40 channels set to zero. Therefore, an optical m-QAM OFDM signals that has 88 subcarriers and occupies a total bandwidth of 7GHz can be generated. And then we use two the same type low noise amplifier to amplify signal-I and signal-Q to reach the best modulation index (MI) condition. Following, we use tunable phase shift to control $90^0$ phase delay between signal-I and signal-Q. In order to realize optical direct-detection OFDM signal, a new optical subcarrier is generated at the lower sideband of the original carrier by 12GHz. In there, we use a $90^0$ phase delay coupler to divide the sinusoidal wave into two parts. And combine the OFDM signals and clock signal. Then we bias both MZ-a and MZ-b at null point and set the phase modulator to delay $90^0$. After the first MZM, the generated OFDM signals is up-converted by using frequency quadrupling technique. After 50/100 optical inter-leaver to filter out the sideband we don't want, the OFDM signals at 60GHZ is generated at (a) of Fig 4-1. A 25-km single mode fiber (SMF) is used

to evaluate the transmission penalty of the system. After square-law photo diode (PD) detection, an electrical OFDM signals at 60GHz is generated and down-converted to 5GHz at (b) of Fig 4-2. The down-converted OFDM signals is captures by a Tektronix® DPO 71254 with a 50GHz sample rate and a 3-dB bandwidth of 12.5GHz. An off-line DSP program is employed to demodulate the OFDM signal. The demodulation process includes synchronization, Fast Fourier Transform (FFT), one-tap equalization, I/Q imbalance compensation and QAM symbols decoding. The bit error rate (BER) performance is calculated from the measured signal-to-noise ratio (SNR).

## 4.3 Experimental results for OFDM signal without bit-loading algorithms

The equalizer in OFDM transceiver is used to combat both frequency response of various millimeter-wave components at 60GHz and fiber dispersion. Since the proposed OFDM transmitter can generate high-purity two-tone light-wave, the generated OFDM signals do not suffer from periodic fading issue due to fiber dispersion. Only in-band distortion of the OFDM-encoded subcarrier induced by fiber dispersion is considered. Since the symbol rate of each subcarrier is only 78.125MSym/s, the fiber chromatic penalty can be ignored.

### 4.3.1 Optimal condition for 8-QAM OFDM signal

The relative intensity between optical un-modulated and data-modulated subcarriers strongly influences the performance of the optical OFDM signals. One of the advantages of the proposed OFDM transmitter is that relative

intensity between optical un-modulated and data-modulated subcarriers can be easily tuned by adjusting the individual amplitude of the driving sinusoidal and OFDM signals to optimize the performance of the direct-detection OFDM signals, respectively.

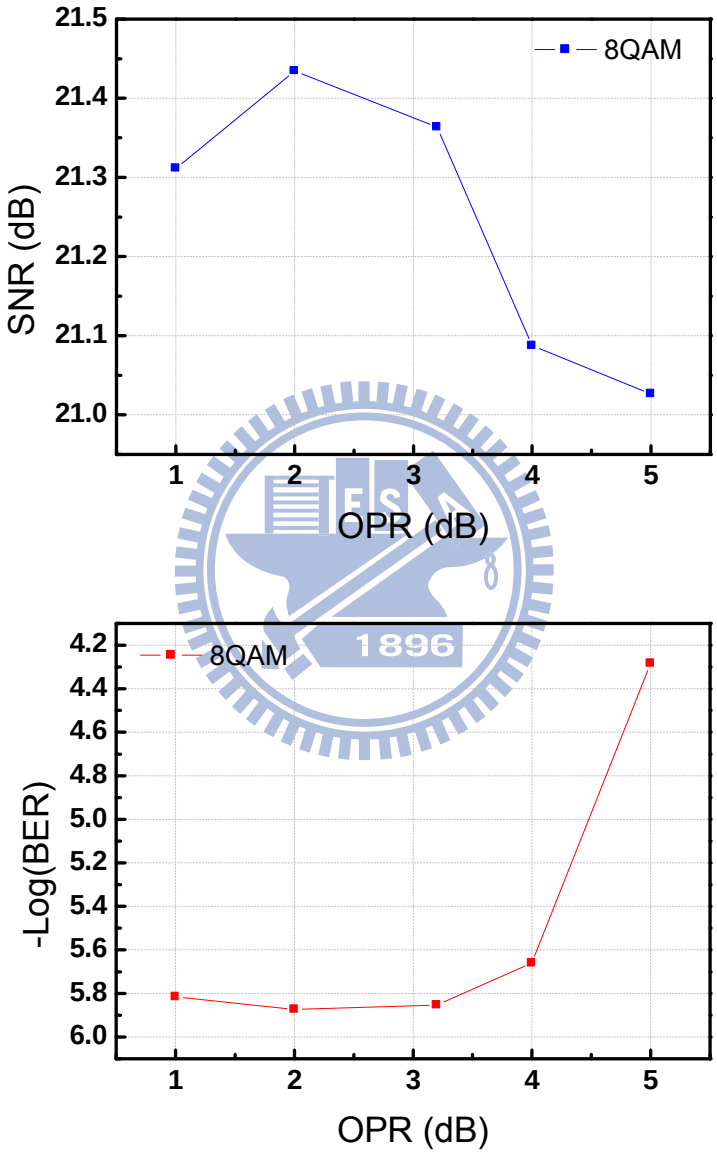


Figure 4-2 SNR and BER vs. OPR for 8-QAM OFDM signal.

Figure 4-2 illustrates the SNR and BER of the 8-QAM OFDM signals versus different optical power ratios (OPR) of the um-modulated subcarrier to

the OFDM-encoded subcarrier as optical power of 60-GHz OFDM signals are normalized before detection. The optimal OPR is 2 dB.

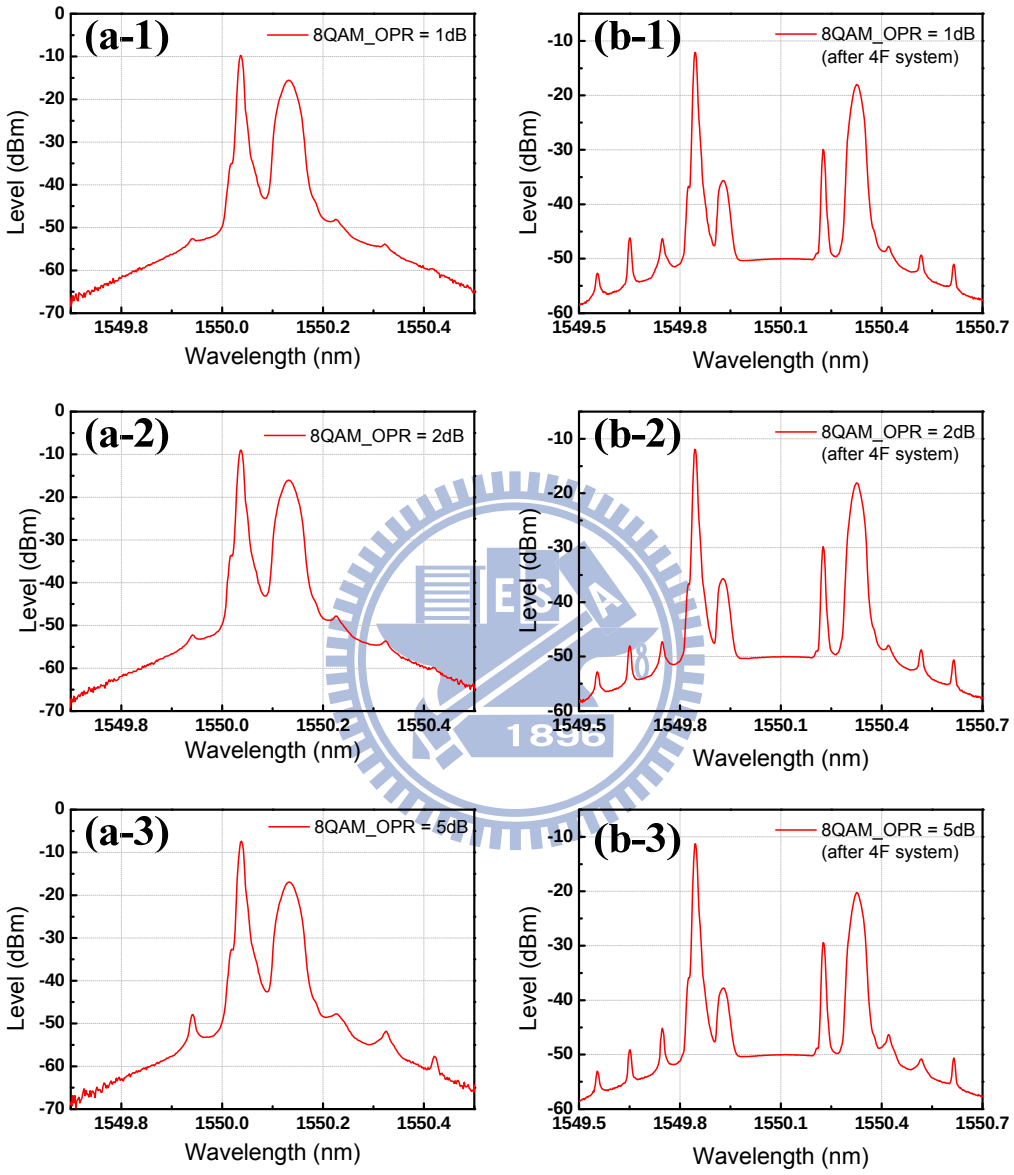


Figure 4-3 Optical spectrums for 8-QAM OFDM signal.

Figure 4-3 shows the optical spectrums of different OPR. We define OPR is optical power of un-modulated subcarrier over power of signals modulated optical carrier. And inset (a-1), (a-2), (a-3) of Fig. 4-3 are OPR = 1 dB, OPR =

2 dB, OPR = 5 dB before frequency quadrupling system, respectively. Inset (b-1), (b-2) and (b-3) illustrate OPR = 1 dB, OPR = 2 dB, OPR = 5 dB after frequency quadrupling system and interleaver.

### 4.3.2 Optimal condition for 16-QAM OFDM signal

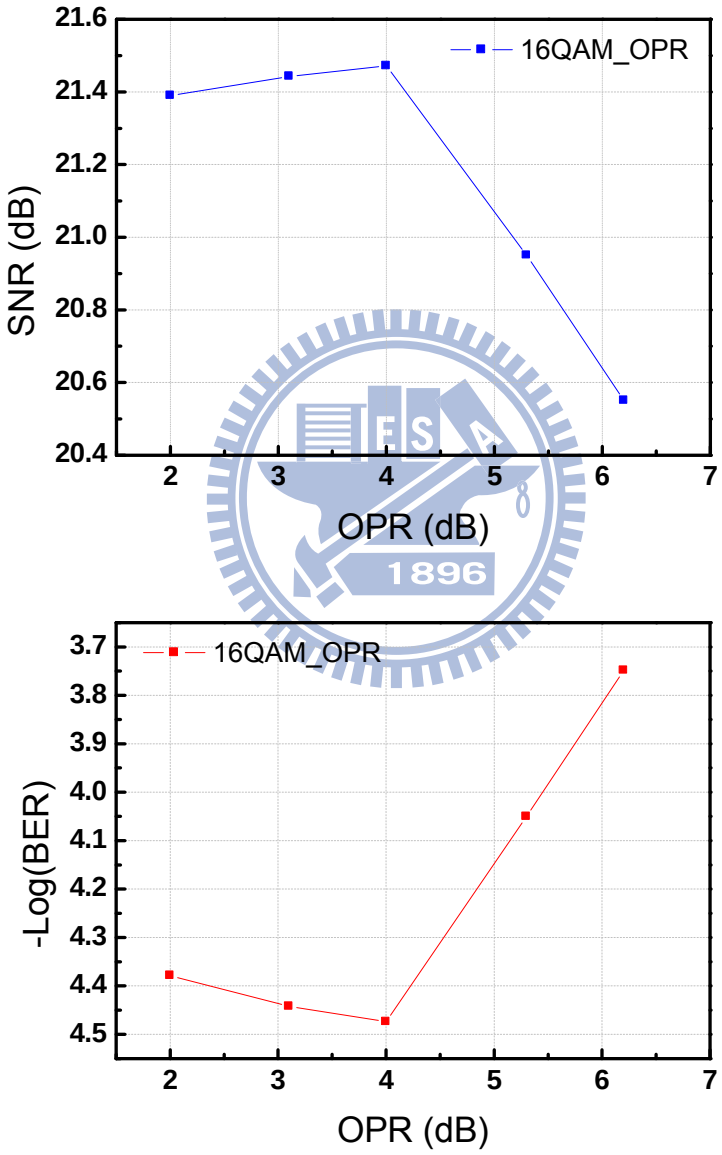


Figure 4-4 SNR and BER vs. OPR for 16-QAM OFDM signal.

Figure 4-4 illustrates the SNR and BER of the 16-QAM OFDM signals

versus different optical power ratios (OPR) of the um-modulated subcarrier to the OFDM-encoded subcarrier as optical power of 60-GHz OFDM signals are normalized before detection. The optimal OPR is 4 dB.

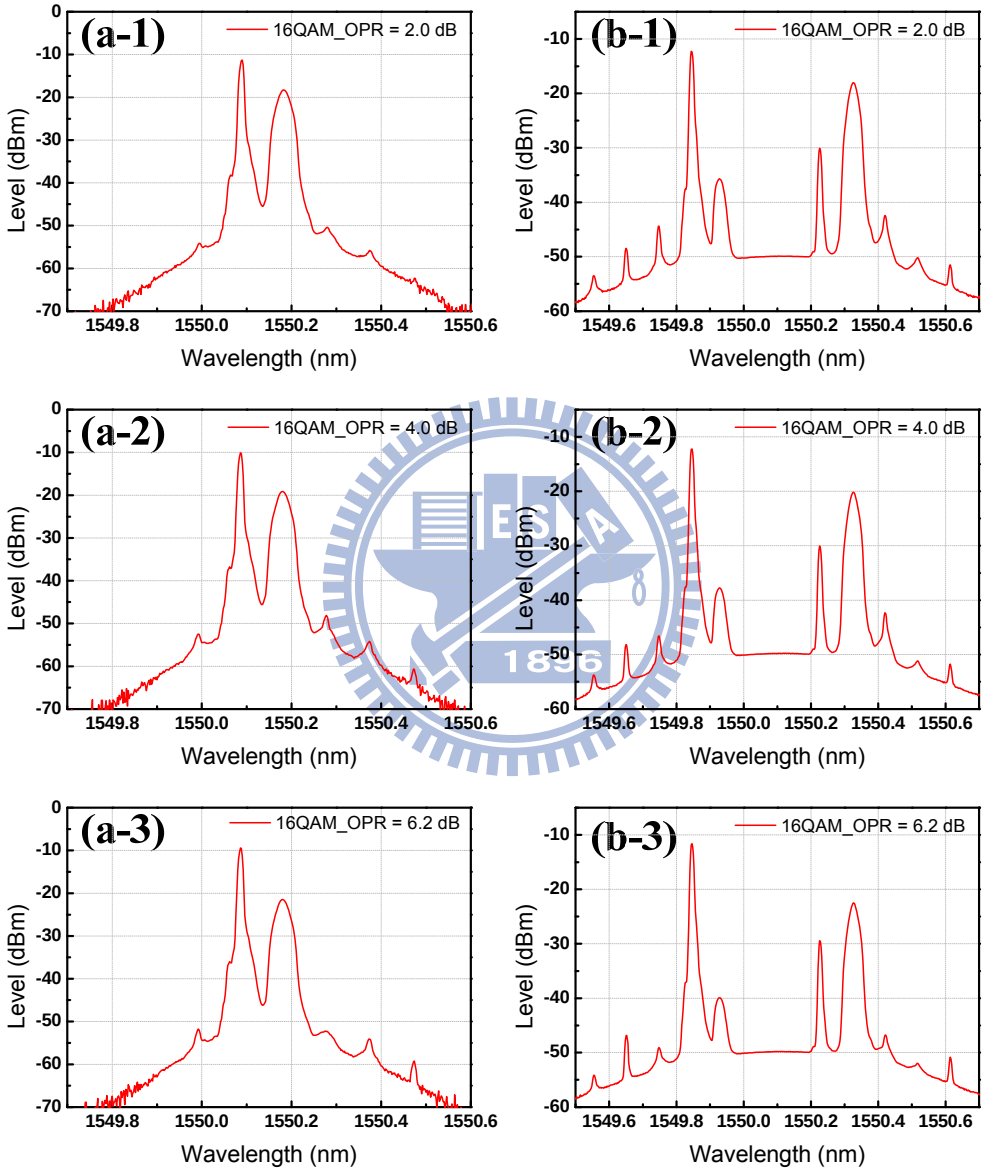


Figure 4-5 Optical spectrums for 16-QAM OFDM signal.

Figure 4-5 shows the optical spectrums of different OPR. And inset (a-1), (a-2), (a-3) of Fig. 4-5 are OPR = 2dB, OPR = 4 dB, OPR = 6.2 dB before

frequency quadrupling system, respectively. Inset (d), (e) and (f) illustrate OPR = 2 dB, OPR = 4 dB, OPR = 6.2 dB after frequency quadrupling system and interleaver.

### 4.3.3 Optimal condition for 32-QAM OFDM signal

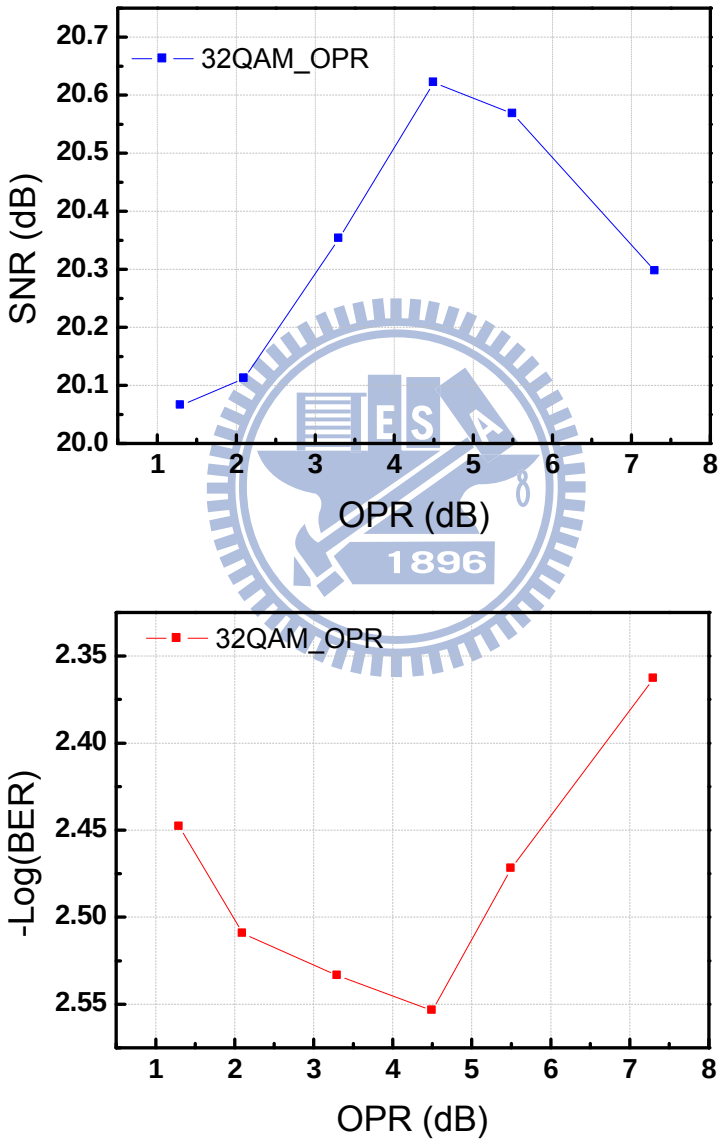


Figure 4-6 SNR and BER vs. OPR for 32-QAM OFDM signal.

Figure 4-6 illustrates the SNR and BER of the 32-QAM OFDM signals

versus different optical power ratios (OPR) of the um-modulated subcarrier to the OFDM-encoded subcarrier as optical power of 60-GHz OFDM signals are normalized before detection. The optimal OPR is 4.5 dB.

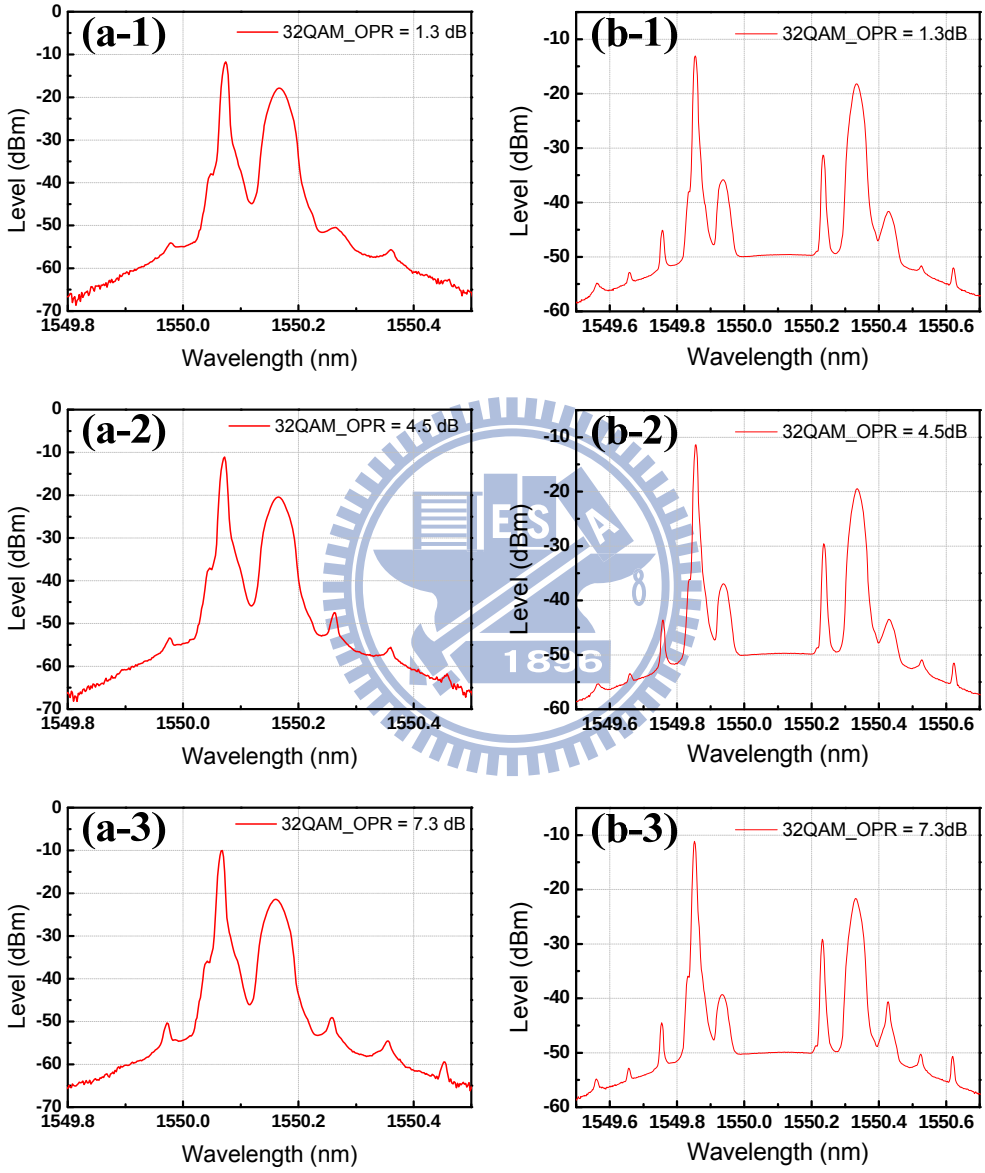


Figure 4-7 Optical spectrums for 32-QAM OFDM signal.

Figure 5-11 shows the optical spectrums of different OPR. And inset (a-1), (a-2), (a-3) of Fig. 4-7 are OPR = 1.3 dB, OPR = 4.5 dB, OPR = 7.3 dB before

frequency quadrupling system, respectively. Inset (b-1), (b-2) and (b-3) illustrate OPR = 1.3 dB, OPR = 4.5 dB, OPR = 7.3 dB after frequency quadrupling system and interleaver.

### 4.3.4 Transmission results of 8-QAM

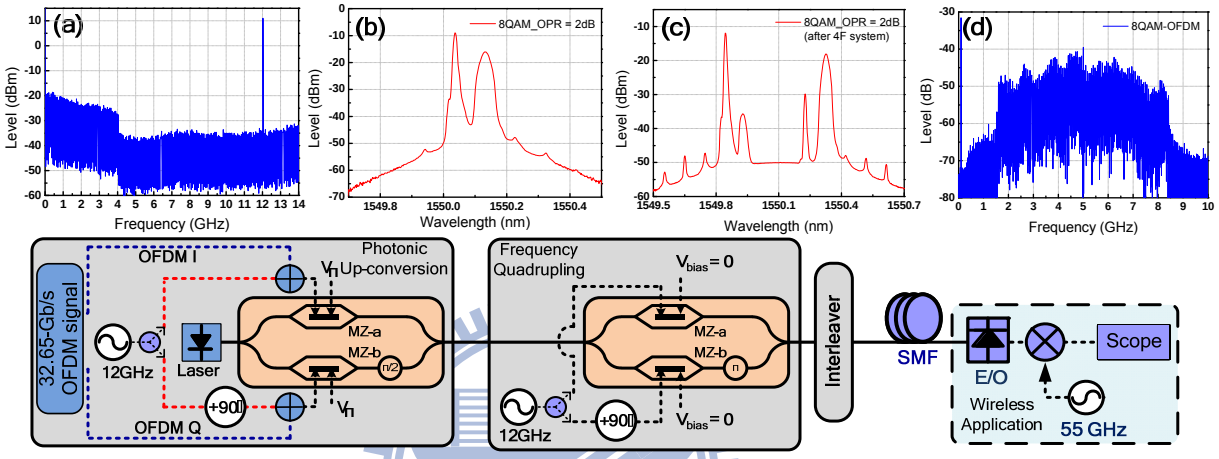


Figure 4-8 Electrical spectrums of 8-QAM OFDM signals.

Figure 4-8 illustrates the electrical spectrums for 8-QAM signals and indicates where the spectrums belong to. Inset (a) of Fig. 4-8 is the electrical spectrum of transmitter terminal OFDM signals and 12-GHz subcarrier. Inset (b) of Fig. 4-8 is the optical spectrum of I/Q up-conversion. Inset (c) of Fig. 4-8 receiver is the optical spectrum of frequency quadrupling. Inset (d) of Fig. 4-8 is the electrical spectrum of 8-QAM OFDM signals. We down-convert the signals to center frequency 5-GHz and the bandwidth is 7-GHz.

Figure 4-9 shows the SNR and BER curves of the 20.625Gbps 8-QAM OFDM signals using optimal OPR after transmission over 25-km SMF. After transmission 25-km, the sensitivity penalties is zero dB. Although it still worsens the performance a little, it does better than using electrical mixer with

noise figure (NF) 8-dB.

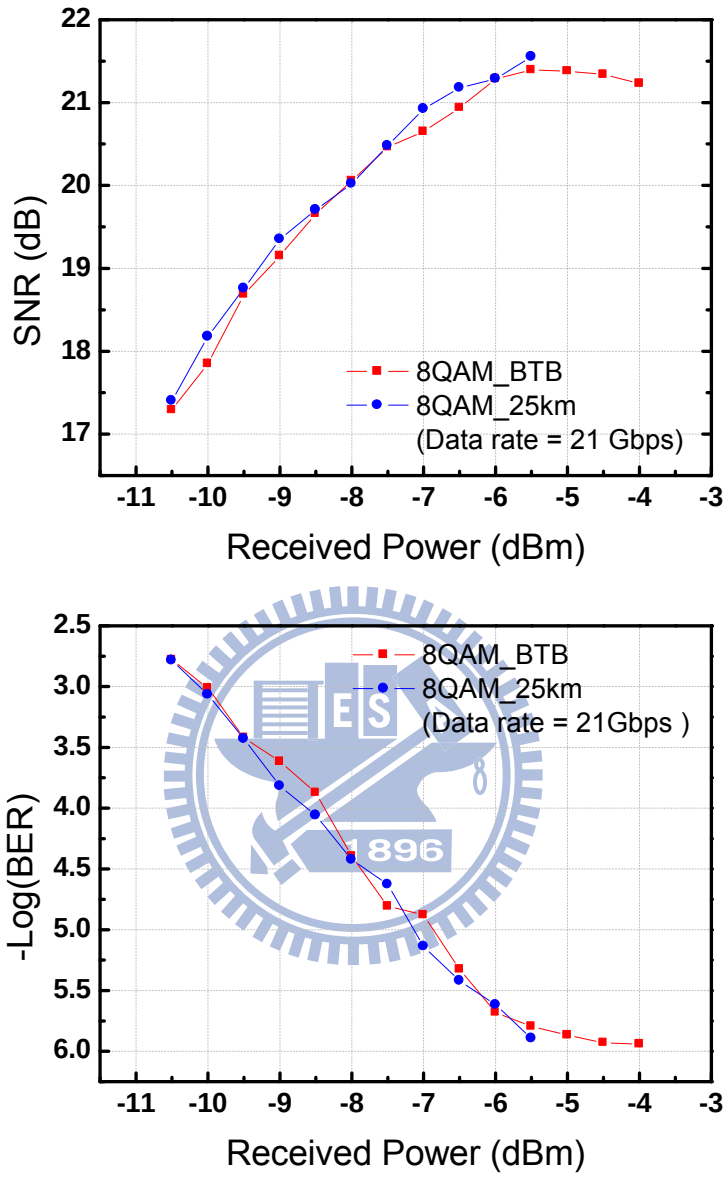


Figure 4-9 SNR and BER vs. Received power for 8-QAM OFDM signal.

Figure 4-10 shows 8-QAM constellation diagrams and Fig. 4-11 shows SNR (and BER) vs. subcarrier number after the system in back-to-back and 25km SMF transmission. They are captured at PD received power equal to -6dBm. The equalizer in OFDM transceiver is used to combat both frequency responses of various millimeter-waves components at 60GHz and fiber

dispersion. Since the OFDM transmitter can generate high-purity two-tone lightwave, the generated OFDM signals do not suffer from periodic fading issue due to fiber dispersion. Only in-band distortion of the OFDM-encoded subcarrier induced by fiber dispersion is considered. Since the symbol rate of each subcarrier is only 78.125 MSym/sec, the fiber chromatic penalty can be ignored.

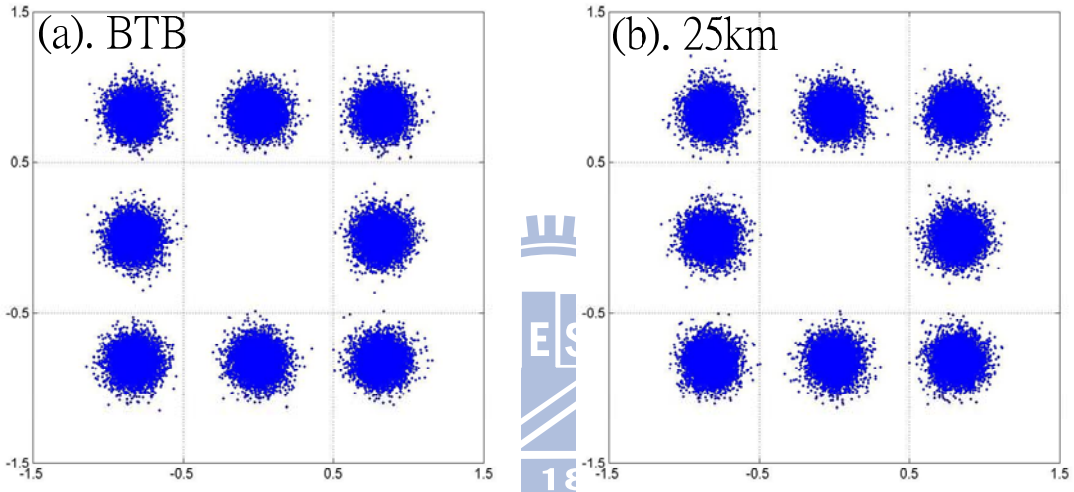


Figure 4-10 Constellations of the 8-QAM OFDM signal.

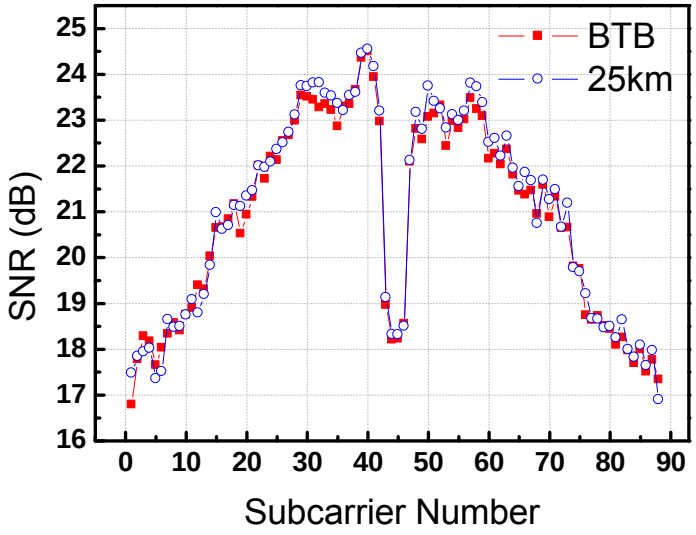


Figure 4-11 (a) SNR vs. Subcarrier Number of the 8-QAM OFDM signal.

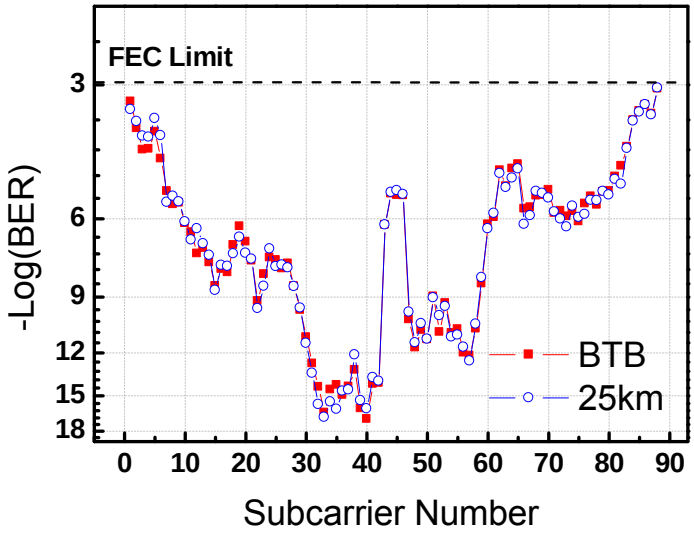


Figure 4-11 (b) BER vs. Subcarrier Number of the 8-QAM OFDM signal.

### 4.3.5 Transmission results of 16-QAM

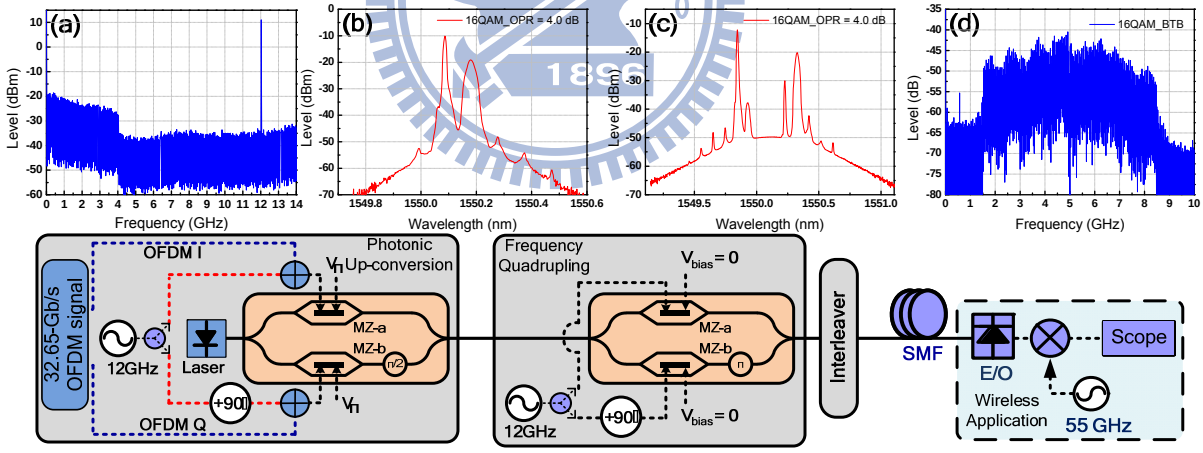


Figure 4-12 Electrical spectrums of 16-QAM OFDM signals.

Figure 4-12 illustrates the electrical spectrums for 16-QAM signals and indicates where the spectrums belong to. Inset (a) of Fig. 4-12 is the electrical spectrum of transmitter terminal OFDM signals and 12-GHz subcarrier. Inset (b) of Fig. 4-11 is the optical spectrum of I/Q up-conversion. Inset (c) of Fig.

4-11 receiver is the optical spectrum of frequency quadrupling. Inset (d) of Fig. 4-11 is the electrical spectrum of 16-QAM OFDM signals. We down-convert the signals to center frequency 5-GHz and the bandwidth is 7-GHz.

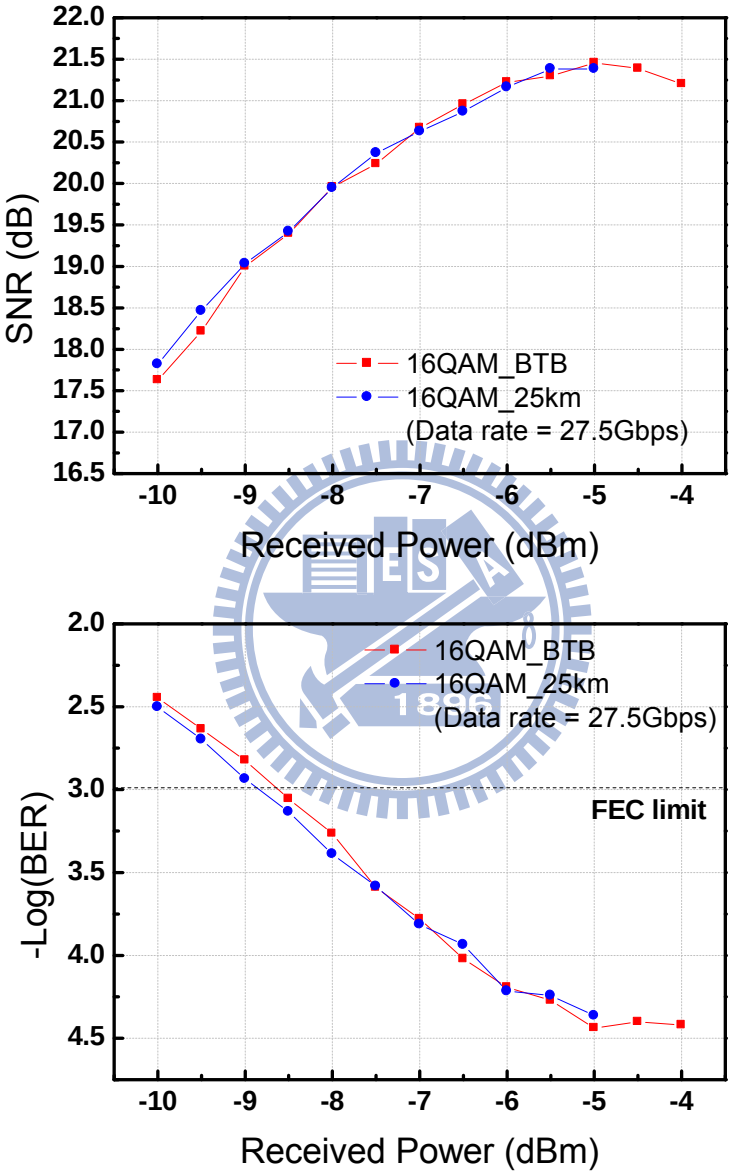


Figure 4-13 SNR and BER vs. Received power for 16-QAM OFDM signal.

Figure 4-13 shows the SNR and BER curves of the 27.5Gbps 16-QAM OFDM signals using optimal OPR after transmission over 25-km SMF. After

transmission 25-km, the sensitivity penalties is zero dB. Although it still worsens the performance a little, it does better than using electrical mixer with noise figure (NF) 8-dB.

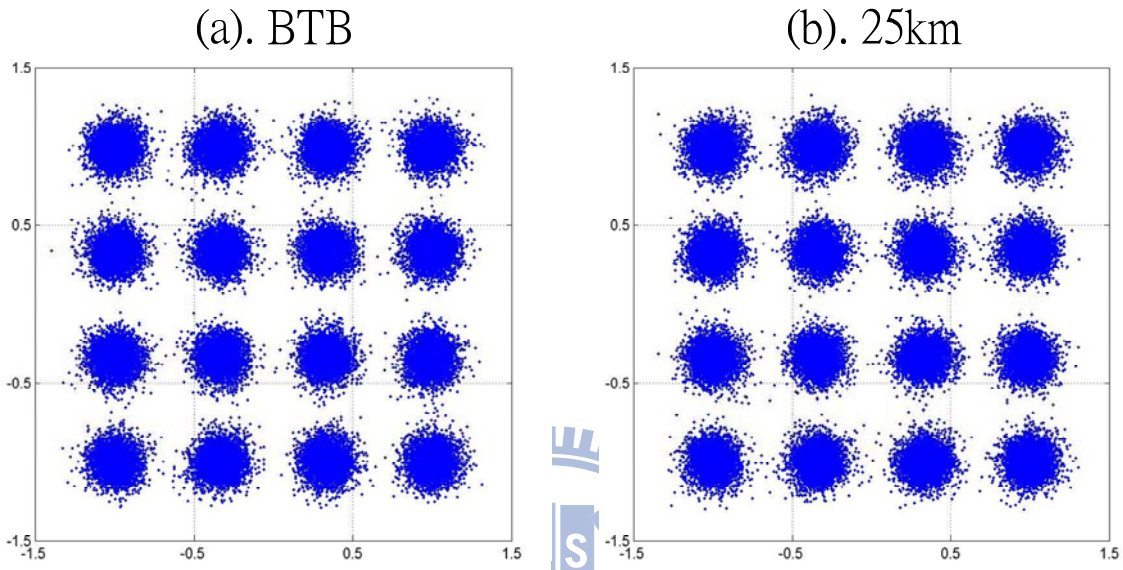


Figure 4-14 Constellations of the 16-QAM OFDM signal.

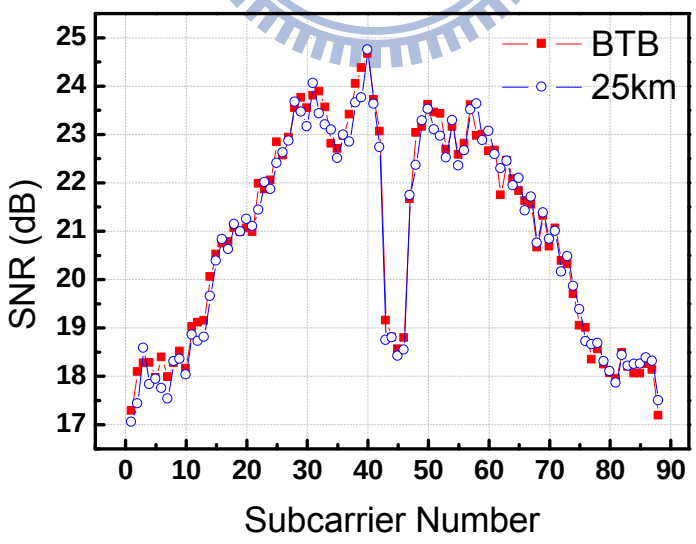


Figure 4-15 (a) SNR vs. Subcarrier Number of the 16-QAM OFDM signal.

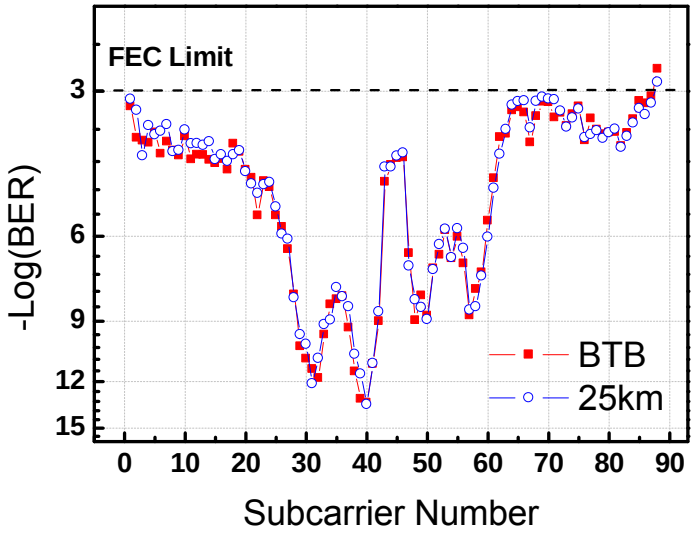


Figure 4-15 (b) BER vs. Subcarrier Number of the 16-QAM OFDM signal.

Figure 4-14 shows 16-QAM constellation diagrams and Fig 4.15 shows SNR (and BER) vs. subcarrier number after the system in back-to-back and 25km SMF transmission. They are captured at PD received power equal to -6dBm.

### 4.3.6 Transmission results of 32-QAM

Figure 4-16 illustrates the electrical spectrums for 32-QAM signals and indicates where the spectrums belong to. Inset (a) of Fig. 4-16 is the electrical spectrum of transmitter terminal OFDM signals and 12-GHz subcarrier. Inset (b) of Fig. 4-16 is the optical spectrum of I/Q up-conversion. Inset (c) of Fig. 4-16 receiver is the optical spectrum of frequency quadrupling. Inset (d) of Fig. 4-16 is the electrical spectrum of 32-QAM OFDM signals. We down-convert the signals to center frequency 5-GHz and the bandwidth is 7-GHz.

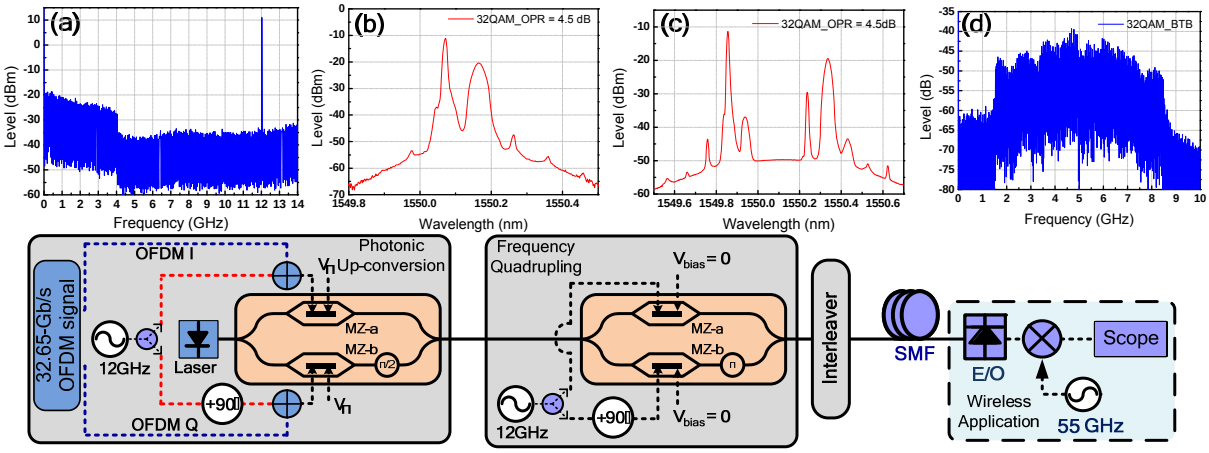


Figure 4-16 Electrical spectrums of 32-QAM OFDM signals.

Figure 4-17 shows the SNR and BER curves of the 34.375Gbps 32-QAM OFDM signals using optimal OPR after transmission over 25-km SMF. After transmission 25-km, the sensitivity penalties is about 0.2dB. Although it still worsens the performance a little, it does better than using electrical mixer with noise figure (NF) 8-dB.

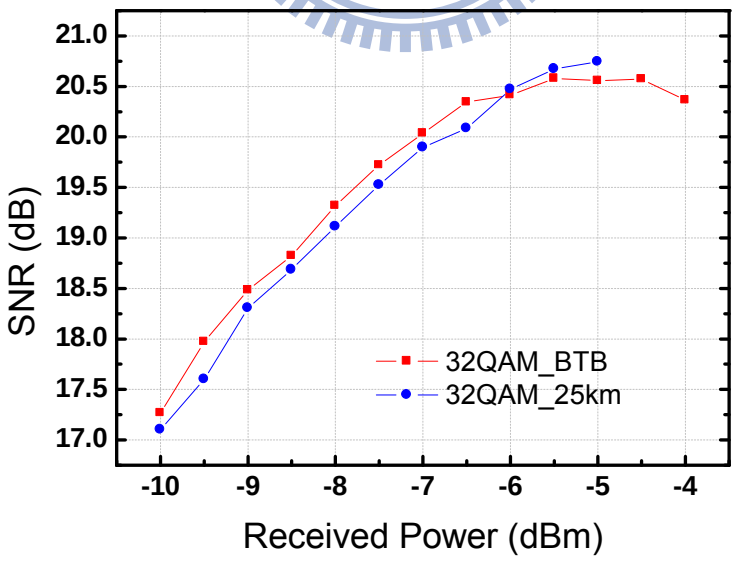


Figure 4-17(a) SNR vs. Received power for 32-QAM OFDM signal.

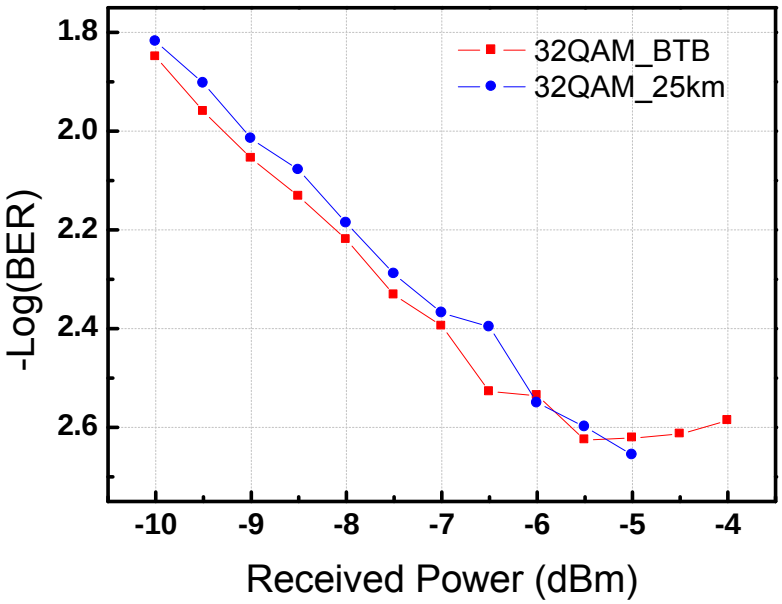


Figure 4-17(b) BER vs. Received power for 32-QAM OFDM signal.

Figure 4-18 shows 32-QAM constellation diagrams and Fig. 4-19 SNR (and BER) vs. subcarrier number after the system in back-to-back and 25km SMF transmission. They are captured at PD received power equal to -6dBm.

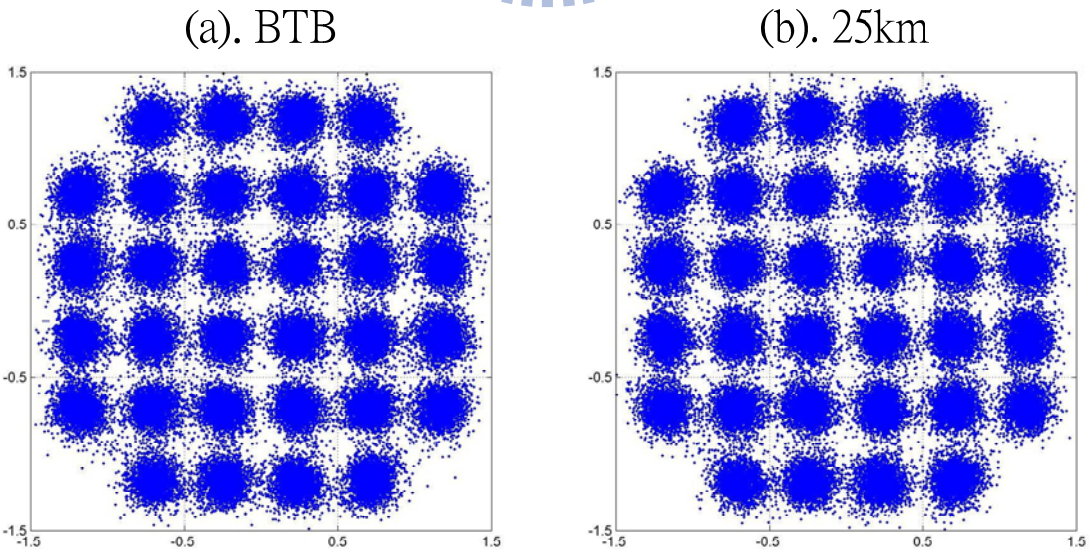


Figure 4-18 Constellations of the 32-QAM OFDM signal.

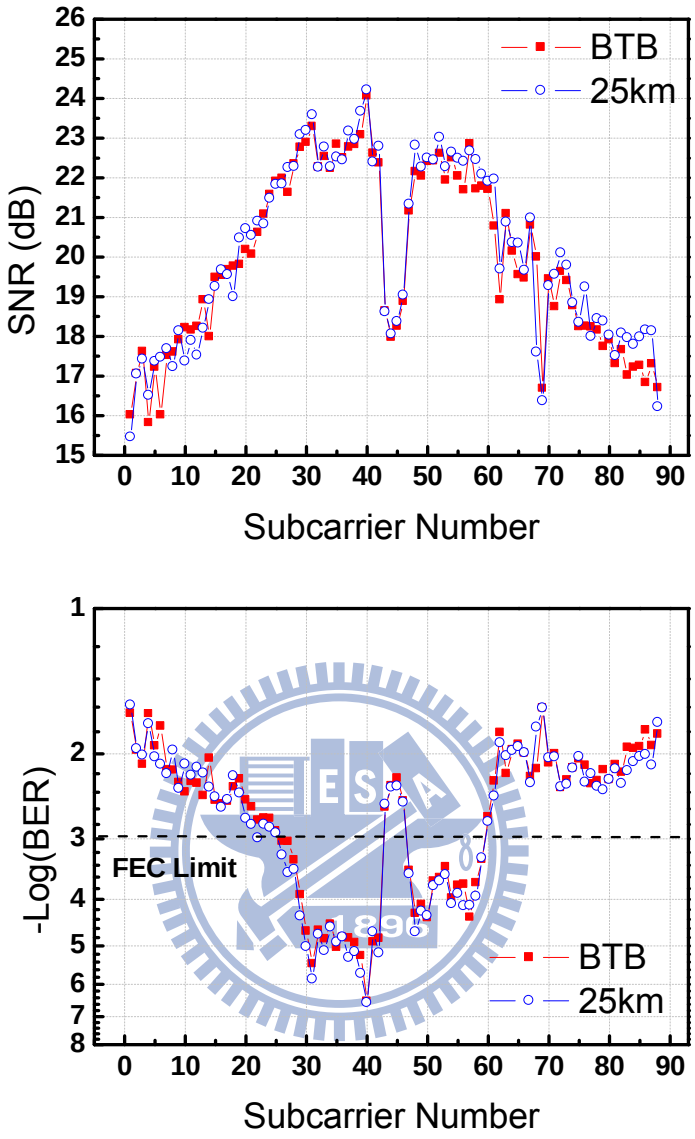


Figure 4-19 SNR and BER vs. Subcarrier Number of the 16-QAM OFDM signal.

## 4.4 Experimental results for OFDM signal with bit-loading algorithms

### 4.4.1 Optimal condition for bit-loading OFDM signal

The relative intensity between optical un-modulated and data-modulated subcarriers strongly influences the performance of the optical OFDM signals.

One of the advantages of the proposed OFDM transmitter is that relative intensity between optical un-modulated and data-modulated subcarriers can be easily tuned by adjusting the individual amplitude of the driving sinusoidal and OFDM signals to optimize the performance of the direct-detection OFDM signals, respectively.

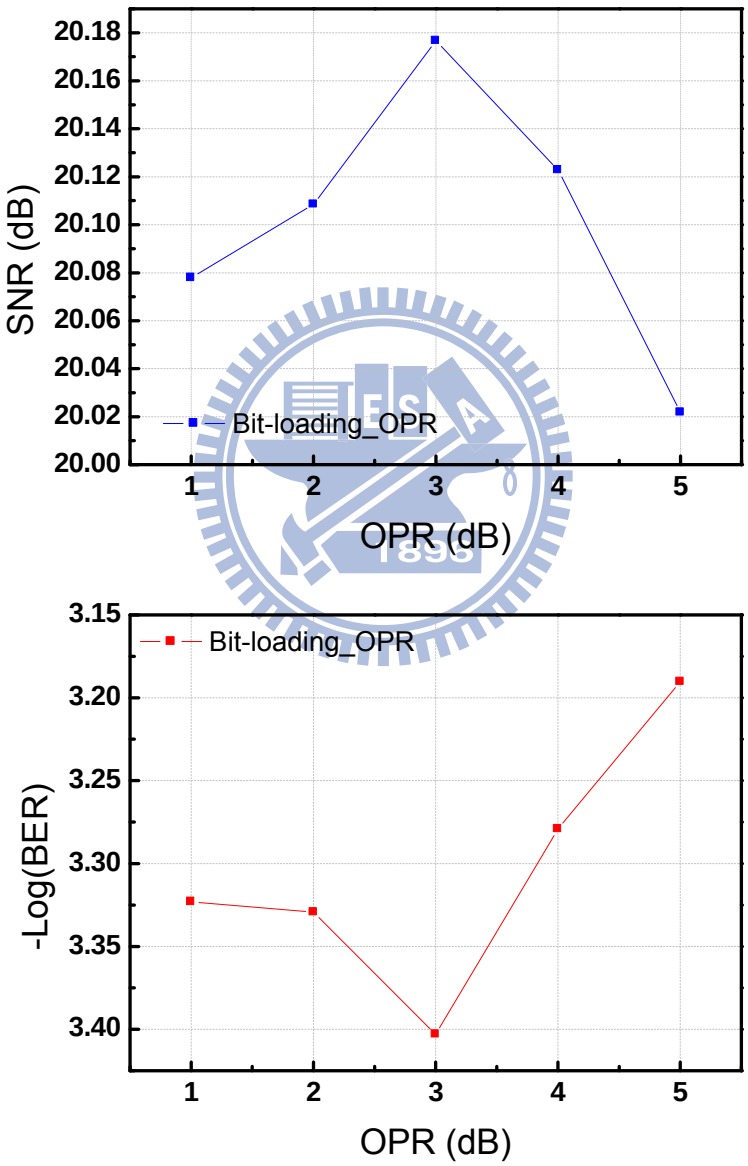


Figure 4-20 SNR and BER vs. OPR for bit-loading OFDM signal.

Figure 4-20 illustrates the SNR and BER of the bit-loading OFDM signals versus different optical power ratios (OPR) of the um-modulated subcarrier to the OFDM-encoded subcarrier as optical power of 60-GHz OFDM signals are normalized before detection. The optimal OPR is 3 dB.

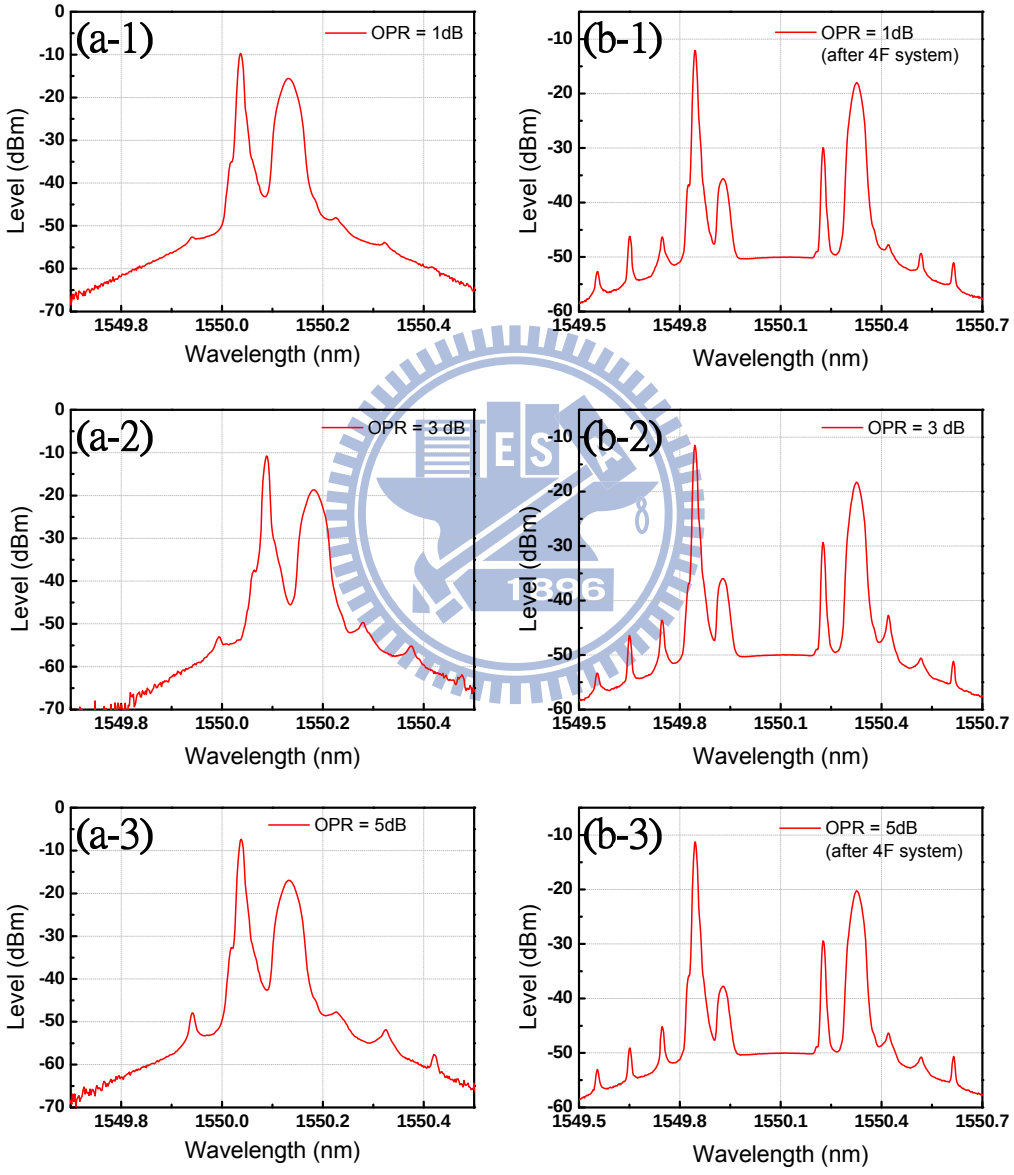


Figure 4-21 Optical spectrums for bit-loading OFDM signal.

Figure 4-21 shows the optical spectrums of different OPR. We define OPR is optical power of un-modulated subcarrier over power of signals modulated optical carrier. And inset (a), (b), (c) of figure 5-5 are OPR = 1 dB, OPR = 3 dB, OPR = 5 dB before frequency quadrupling system, respectively. Inset (d), (e) and (f) illustrate OPR = 1 dB, OPR = 3 dB, OPR = 5 dB after frequency quadrupling system and interleaver.

### 4.4.2 Transmission results of bit-loading OFDM signal

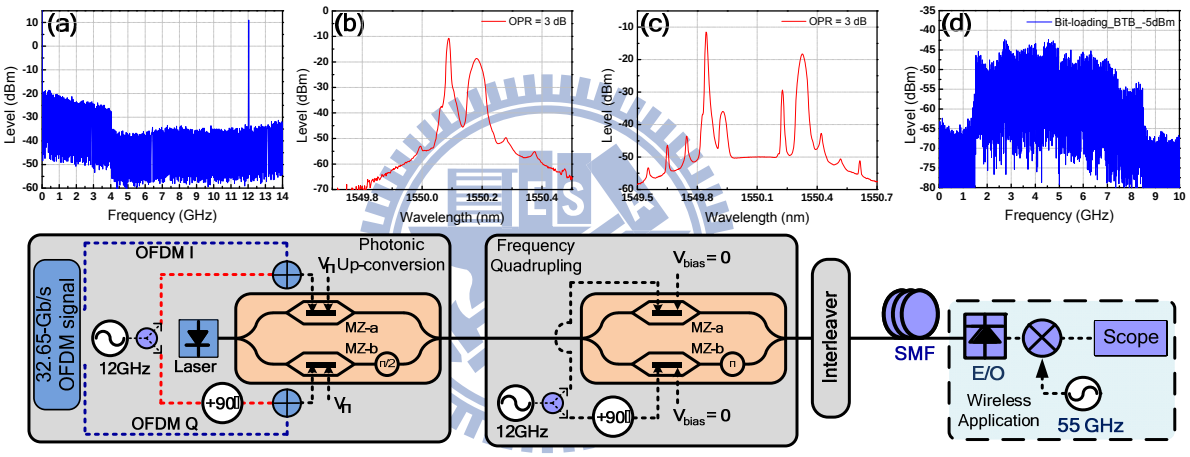


Figure 4-22 Electrical spectrums of bit-loading OFDM signals.

Figure 4-22 illustrates the electrical spectrums for bit-loaidng signals and indicates where the spectrums belong to. Inset (a) of Fig. 4-22 is the electrical spectrum of transmitter terminal OFDM signals and 12-GHz subcarrier. Inset (b) of Fig. 4-22 is the optical spectrum of I/Q up-conversion. Inset (c) of Fig. 4-22 receiver is the optical spectrum of frequency quadrupling. Inset (d) of Fig. 4-22 is the electrical spectrum of bit-loading OFDM signals. We down-convert the signals to center frequency 5-GHz and the bandwidth is 7-GHz.

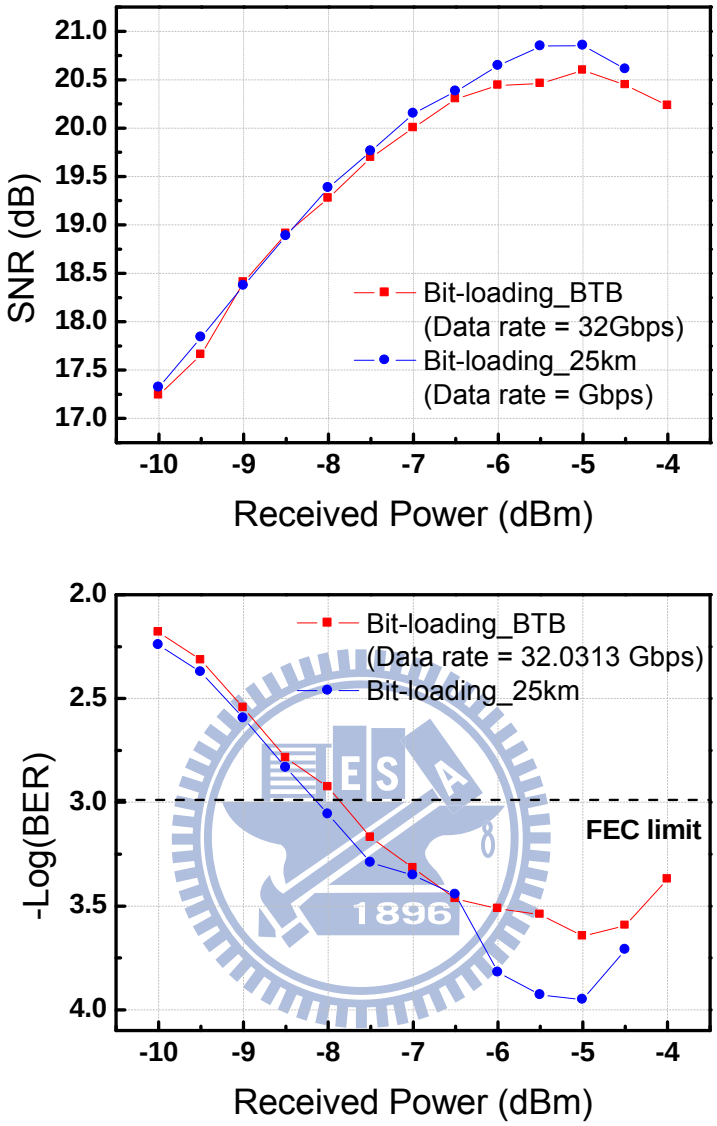


Figure 4-23 SNR and BER vs. Received power for 16-QAM OFDM signal.

Figure 4-23 shows the SNR and BER curves of the 32Gbps bit-loading OFDM signals using optimal OPR after transmission over 25-km SMF. After transmission 25-km, the sensitivity penalties is about 0.3dB. Although it still worsens the performance a little, it does better than using electrical mixer with noise figure (NF) 8-dB.

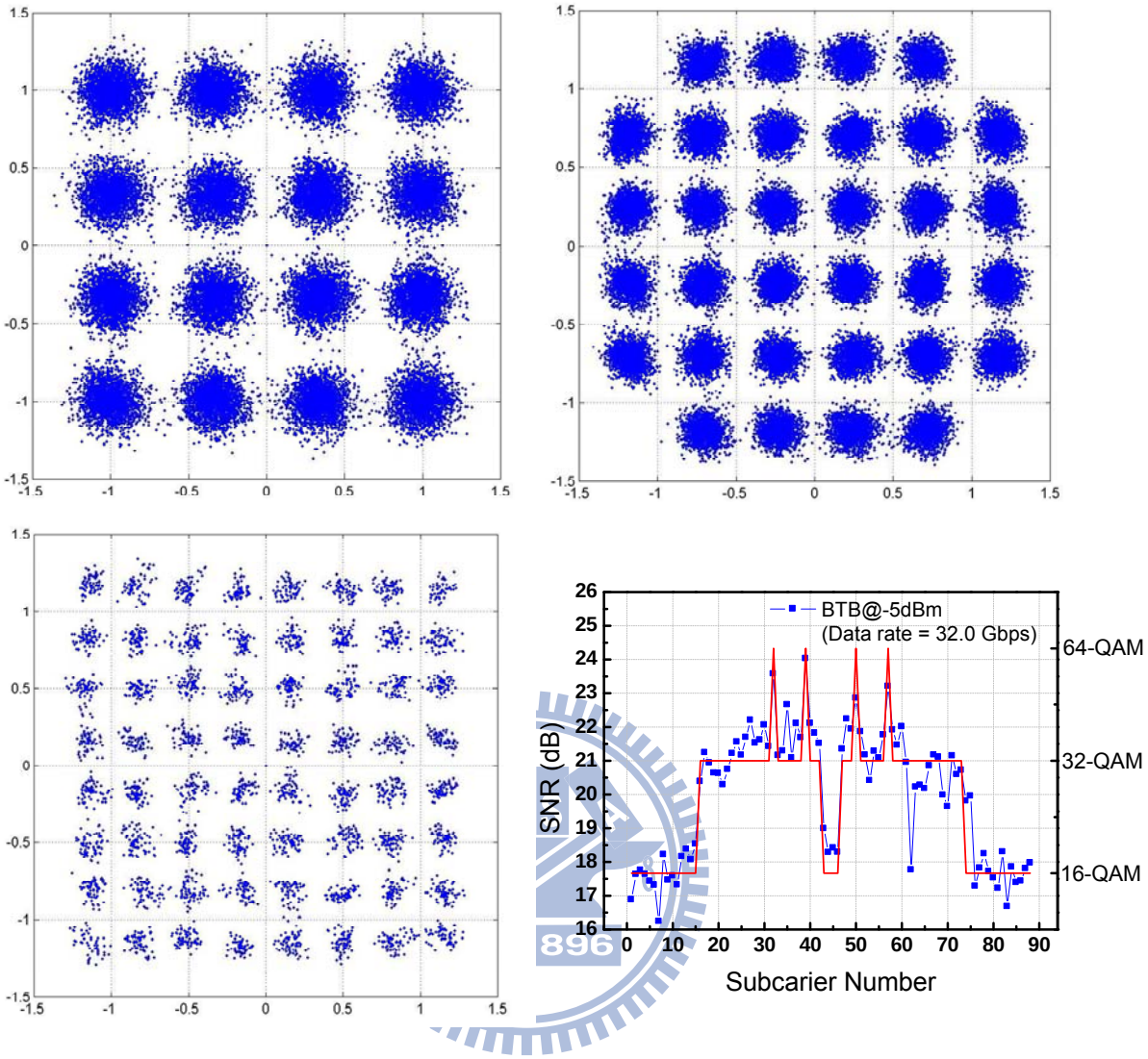


Figure 4-24 Constellations of the bit-loading OFDM signal.

Figure 4-24 shows bit-loading OFDM signals constellation diagrams and SNR vs. subcarrier number after the system in back-to-back and 25km SMF transmission. They are captured at PD received power equal to -6dBm.

Figure 4-25 shows data rate and BER vs. received power after the system in back-to-back and 25km SMF transmission. We fixed BER of each point below then $10^{-3}$. They have different data throughput of received power.

| Fiber Transmission = BTB | | |
|---|---|---|
| Received Power (dBm) | Data rate (Gbit/sec) | BER |
| -5 | 32.0 | 2.79E-04 |
| -6 | 31.1 | 7.84E-04 |
| -7 | 30.3 | 7.40E-04 |
| -8 | 28.9 | 5.15E-04 |
| -9 | 28.1 | 6.37E-04 |

| Fiber Transmission = 25km | | |
|---|---|---|
| Received Power (dBm) | Data rate (Gbit/sec) | BER |
| -5 | 32.0 | 1.16E-04 |
| -6 | 32.0 | 1.04E-04 |
| -7 | 30.3 | 4.79E-04 |
| -8 | 29.4 | 8.39E-04 |
| -9 | 28.3 | 4.18E-04 |

Figure 4-25 (a) Fixed BER of each received power below then $10^{-3}$.

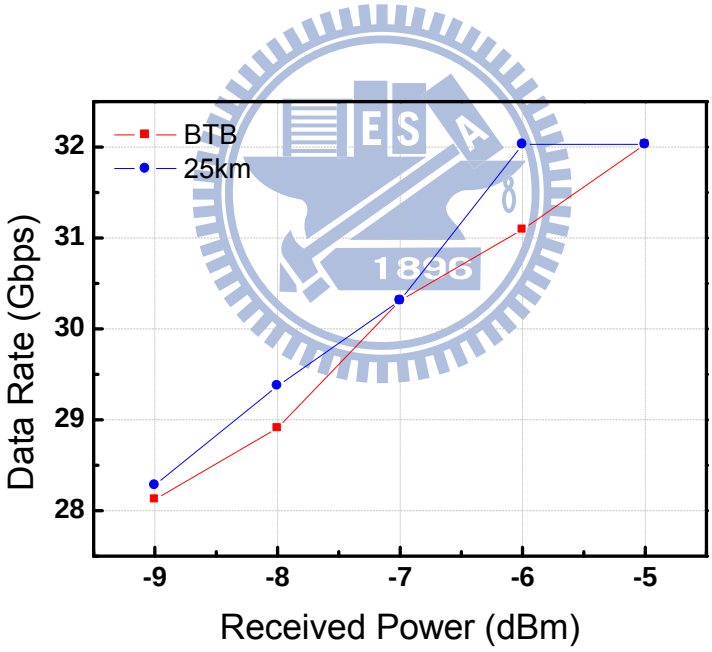


Figure 4-25 (b) Data rate vs. received power of BER below then $10^{-3}$.

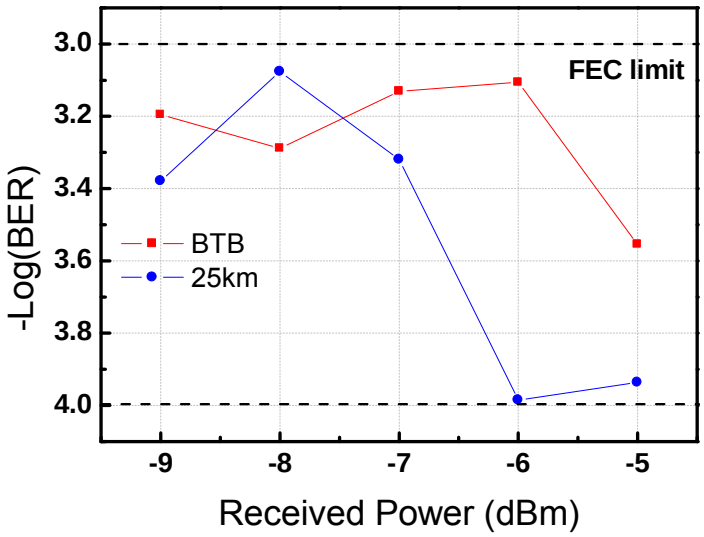


Figure 4-25 (c) BER vs. received power of BER below then $10^{-3}$.

# Chapter 5

## Experimental Demonstration of System for Wireless

### 5.1 Experimental steup

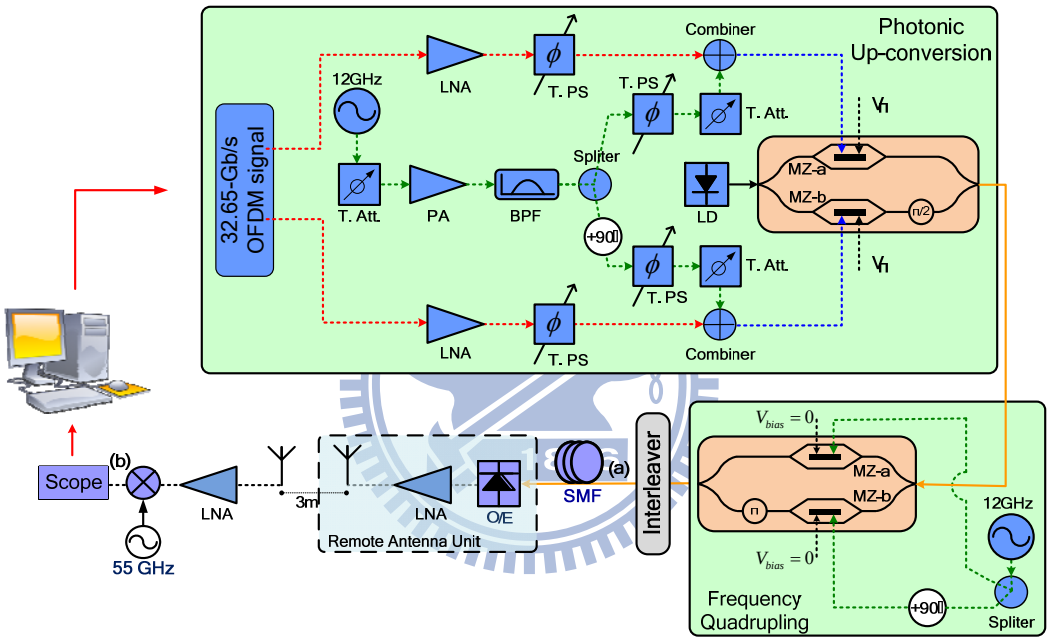


Figure 5-1 Experimental setup for all optical up-conversion with wireless transmission.

Figure 5-3 depicts the experimental setup for all optical I/Q up conversion system via a I/Q modulator. We use a continue wave tunable laser (CW-TL) to generate light source about 1550nm. The light source is then passed through a polarization controller to achieve max optical power when the I/Q modulator is biased at full point. The signals (signal-I and signal-Q) are generated by a Tektronix ® AWG7102 arbitrary waveform generator (AWG) using a

Matlab® program. The sample rate and digital-to-analog converter (DAC) resolution of the AWG are 10 Gb/s and 8 bits, respectively. And we generation four different OFDM signals, 20.625Gb/s 8-QAM OFDM signals, 27.5Gb/s 16-QAM OFDM signals and 34.375Gb/s 32-QAM OFDM signals, all of them have the same parameter, the IFFT length is 128, a 78.125MSyn/s m-QAM symbol is encoded at 88 channels (i.e. channels 2-45 and 85-128) with the remaining 40 channels set to zero. Therefore, an optical m-QAM OFDM signals that has 88 subcarriers and occupies a total bandwidth of 7GHz can be generated. And then we use two the same type low noise amplifier to amplify signal-I and signal-Q to reach the best modulation index (MI) condition. Following, we use tunable phase shift to control $90^0$ phase delay between signal-I and signal-Q. In order to realize optical direct-detection OFDM signal, a new optical subcarrier is generated at the lower sideband of the original carrier by 12GHz. In there, we use a $90^0$ phase delay coupler to divide the sinusoidal wave into two parts. And combine the OFDM signals and clock signal. Then we bias both MZ-a and MZ-b at null point and set the phase modulator to delay $90^0$. After the first MZM, the generated OFDM signals is up-converted by using frequency quadrupling technique. After 50/100 optical inter-leaver to filter out the sideband we don't want, the OFDM signals at 60GHZ is generated at (a) of Figure 5-1. A 25-km single mode fiber (SMF) is used to evaluate the transmission penalty of the system. After square-law photo diode (PD) detection, an electrical OFDM signals at 60GHz is generated and down-converted to 5GHz at (b) of Figure 5-1. The down-converted OFDM signals is captures by a Tektronix® DPO 71254 with a 50GHz sample rate and a 3-dB bandwidth of 12.5GHz. An off-line DSP program is employed to demodulate the OFDM signal. The demodulation process includes

synchronization, Fast Fourier Transform (FFT), one-tap equalization, I/Q imbalance compensation and QAM symbols decoding. The bit error rate (BER) performance is calculated from the measured signal-to-noise ratio (SNR).

## 5.2 Experimental results for OFDM signal without bit-loading algorithms

### 5.2.1 Transmission results of 8-QAM

Figure 5-2 illustrates the electrical spectrums for 8-QAM signals and indicates where the spectrums belong to. Inset (a) of Fig. 5-2 is the electrical spectrum of 8-QAM OFDM signals. We down-convert the signals to center frequency 5-GHz and the bandwidth is 7-GHz.

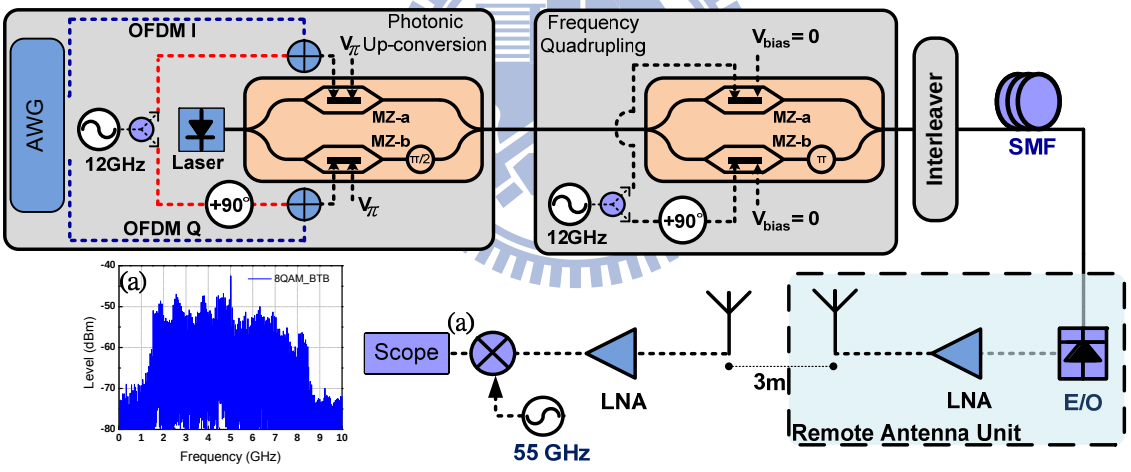


Figure 5-2 Electrical spectrums of 8-QAM OFDM signals with wireless transmission.

Figure 5-3 shows the SNR and BER curves of the 20.625Gbps 8-QAM OFDM signals using optimal OPR after transmission over 25-km SMF. After transmission 25-km, the sensitivity penalties is about 0.3dB. Although it still worsens the performance a little, it does better than using electrical mixer with noise figure (NF) 8-dB.

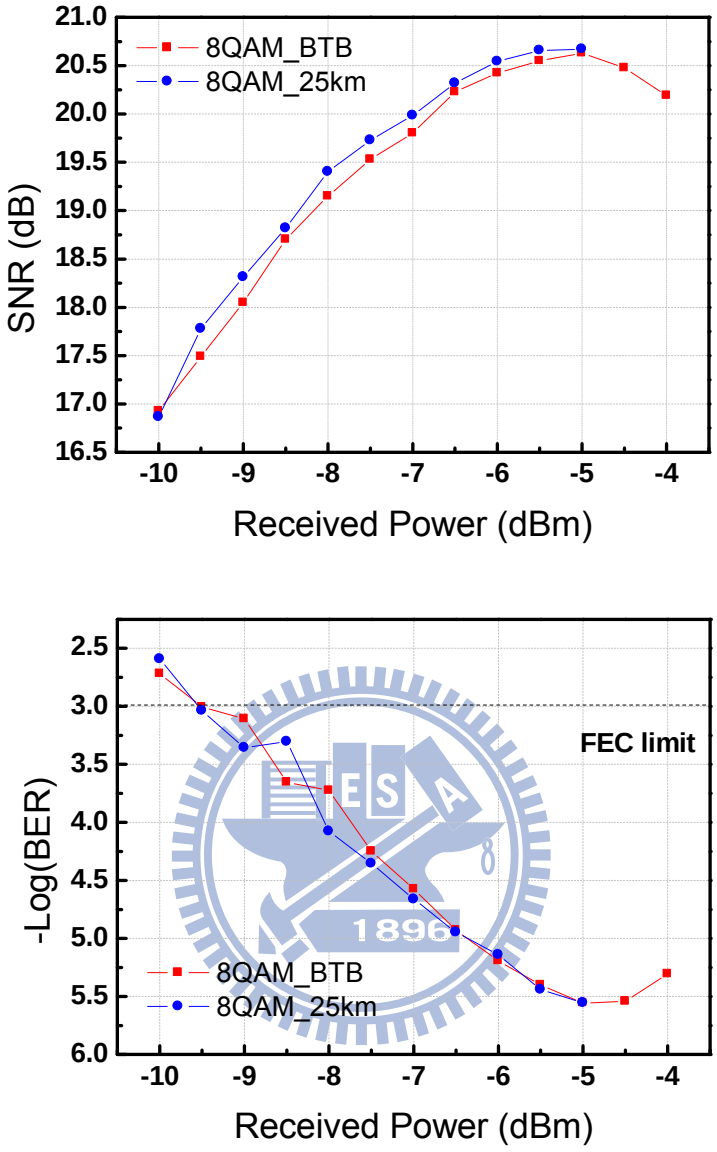


Figure 5-3 SNR and BER vs. Received power for 8-QAM OFDM signal with wireless transmission.

Figure 5-4 shows 8-QAM constellation diagrams and SNR vs. subcarrier number after the system in back-to-back and 25km SMF transmission. They are captured at PD received power equal to -6dBm.

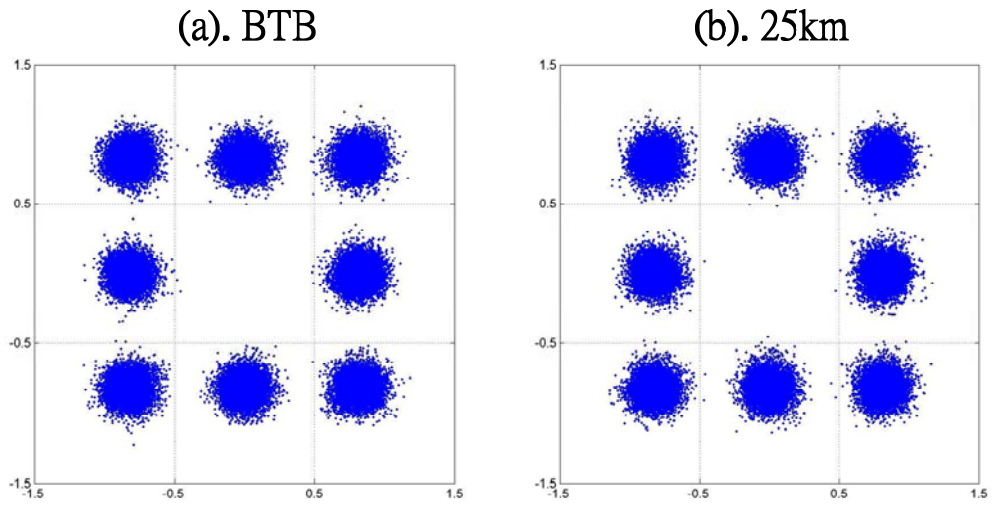


Figure 5-4 (a) Constellations of the 8-QAM OFDM signal with wireless transmission.

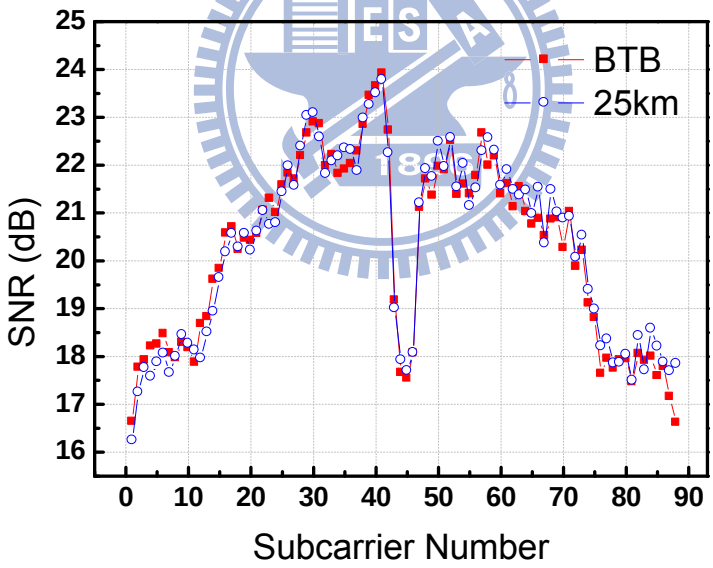


Figure 5-4 (b) SNR vs. Subcarrier Number of the 8-QAM OFDM signal with wireless transmission.

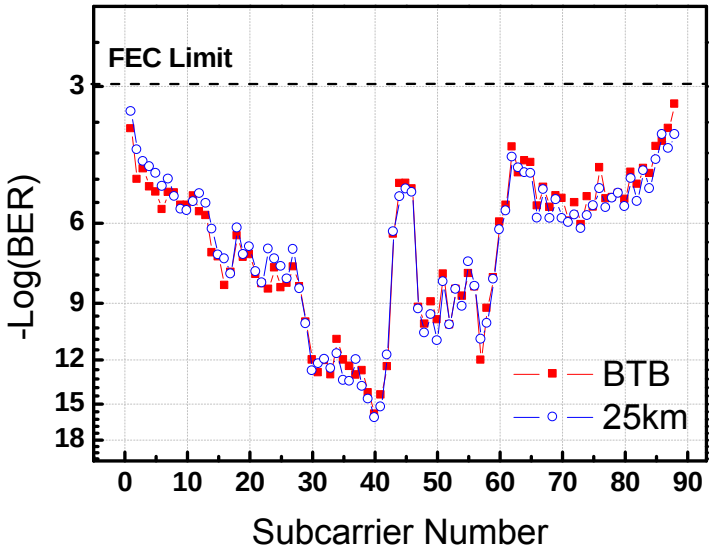


Figure 5-4 (c) BER vs. Subcarrier Number of the 8-QAM OFDM signal with wireless transmission.

### 5.2.2 Transmission results of 16-QAM

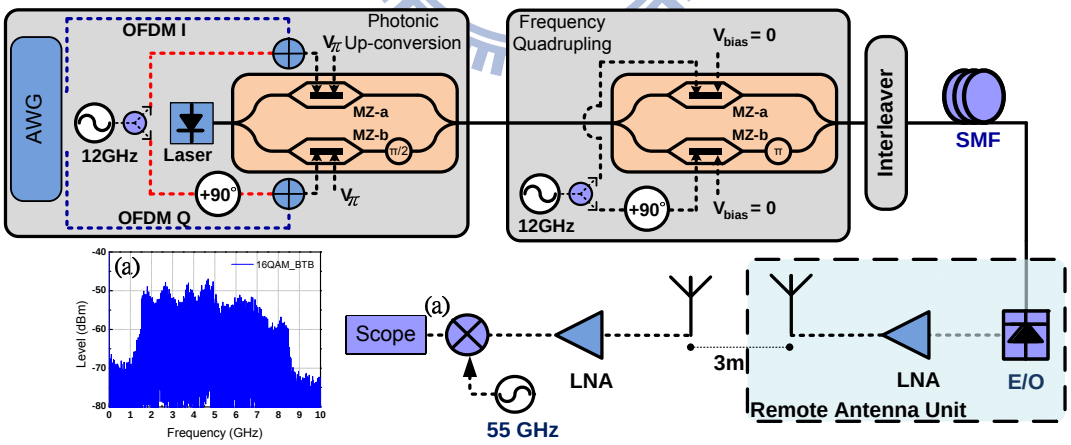


Figure 5-5 Electrical spectrums of 16-QAM OFDM signals with wireless transmission.

Figure 5-5 illustrates the electrical spectrums for 16-QAM signals and indicates where the spectrums belong to. Inset (a) of Fig. 5-5 is the electrical

spectrum of 16-QAM OFDM signals. We down-convert the signals to center frequency 5-GHz and the bandwidth is 7-GHz.

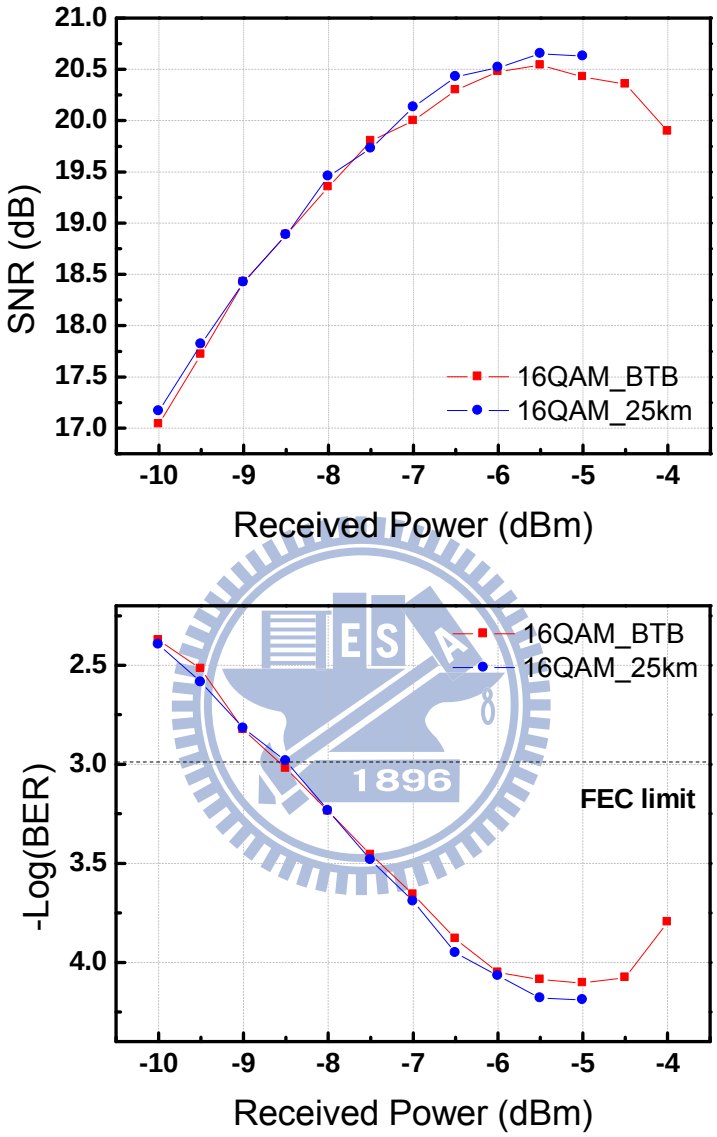


Figure 5-6 SNR and BER vs. Received power for 8-QAM OFDM signal with wireless transmission.

Figure 5-6 shows the SNR and BER curves of the 27.5Gbps 16-QAM OFDM signals using optimal OPR after transmission over 25-km SMF. After transmission 25-km, the sensitivity doesn't have penalties. Although it still

worsens the performance a little, it does better than using electrical mixer with noise figure (NF) 8-dB.

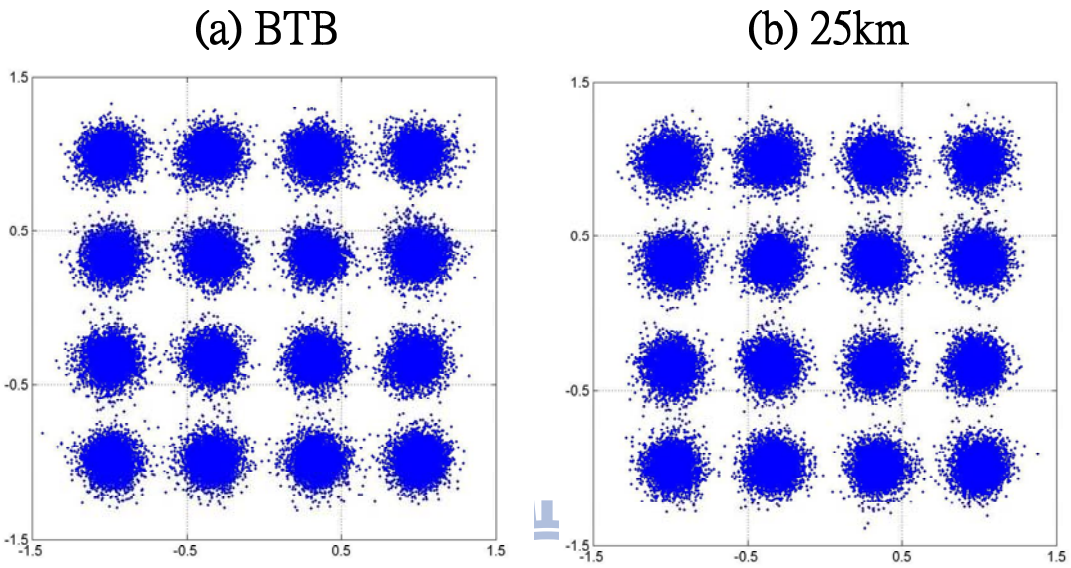


Figure 5-7 (a) Constellation for 8-QAM OFDM signal with wireless transmission.

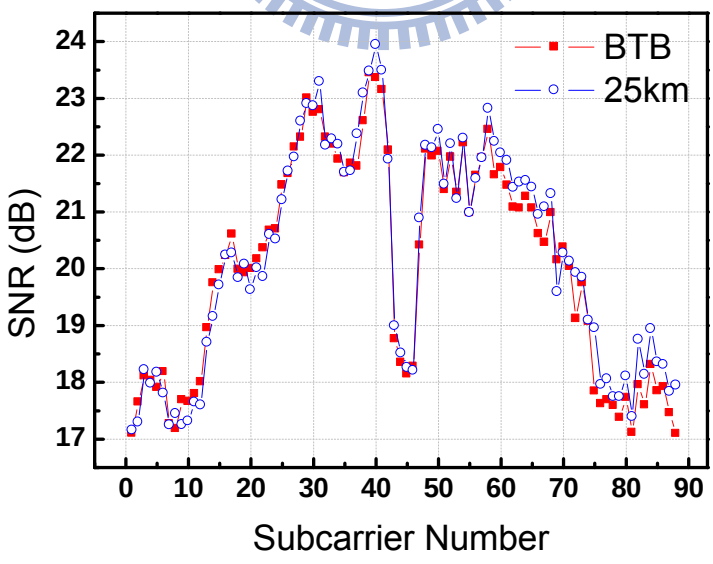


Figure 5-7 (b) SNR vs. Subcarrier Number for 8-QAM OFDM signal with wireless transmission.

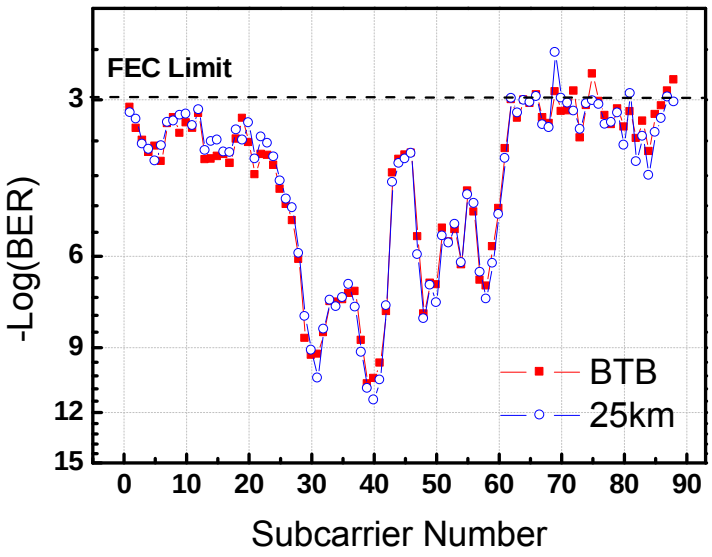


Figure 5-7 (c) BER vs. Subcarrier Number for 8-QAM OFDM signal with wireless transmission.

Figure 5-7 shows 16-QAM constellation diagrams and SNR vs. subcarrier number after the system in back-to-back and 25km SMF transmission. They are captured at PD received power equal to -6dBm.

## 5.3 Experimental results for OFDM signal with bit-loading algorithms

### 5.3.1 Transmission results of bit-loading algorithm

Figure 5-8 illustrates the electrical spectrums for bit-loading OFDM signals and indicates where the spectrums belong to. Inset (a) of Fig. 5-8 is the electrical spectrum of receiver 32-QAM OFDM signals. We down-convert the signals to center frequency 5-GHz and the bandwidth is 7-GHz.

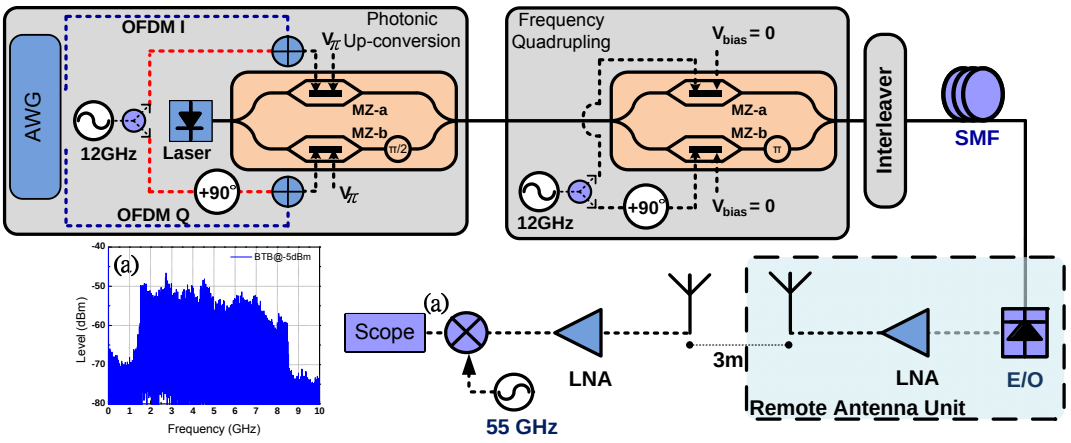


Figure 5-8 Electrical spectrums of Bit-loading OFDM signals with wireless transmission.

Figure 5-9 shows the SNR and BER curves of the bit-loading OFDM signals using optimal OPR after transmission over 25-km SMF. After transmission 25-km, the sensitivity penalties is about 1dB. Although it still worsens the performance a little, it does better than using electrical mixer with noise figure (NF) 8-dB.

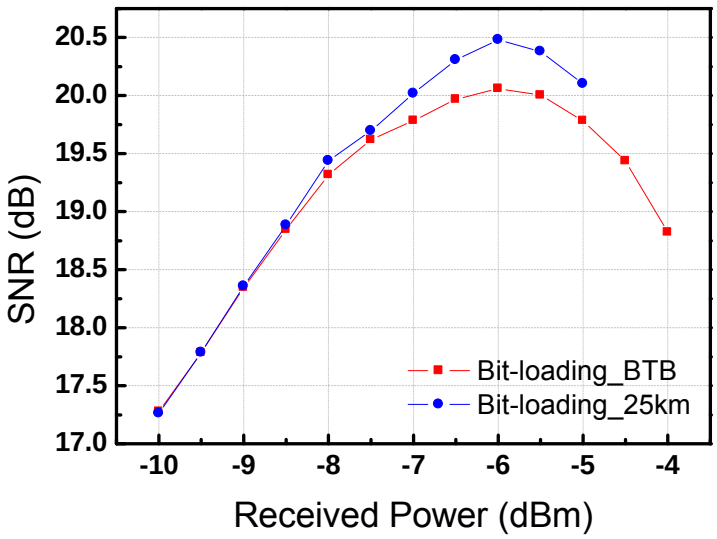


Figure 5-9 (a) SNR vs. Received power for Bit-loading OFDM signal with wireless transmission.

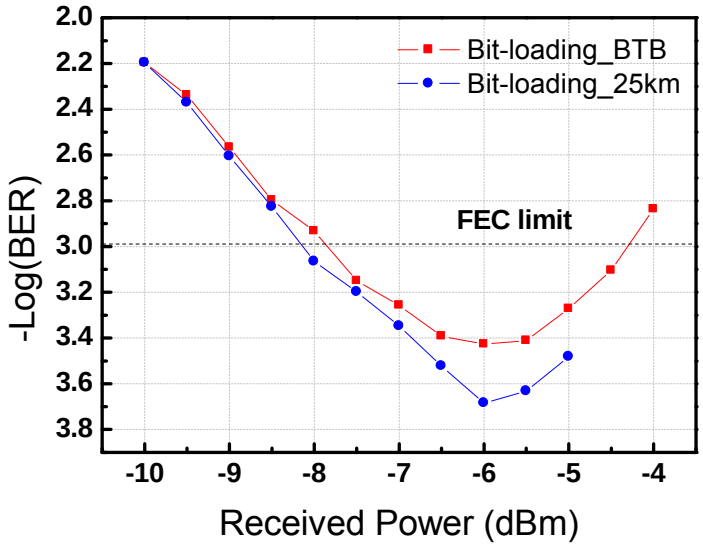


Figure 5-9 (b) BER vs. Received power for Bit-loading OFDM signal with wireless transmission.

**(a) BTB@-5dBm**

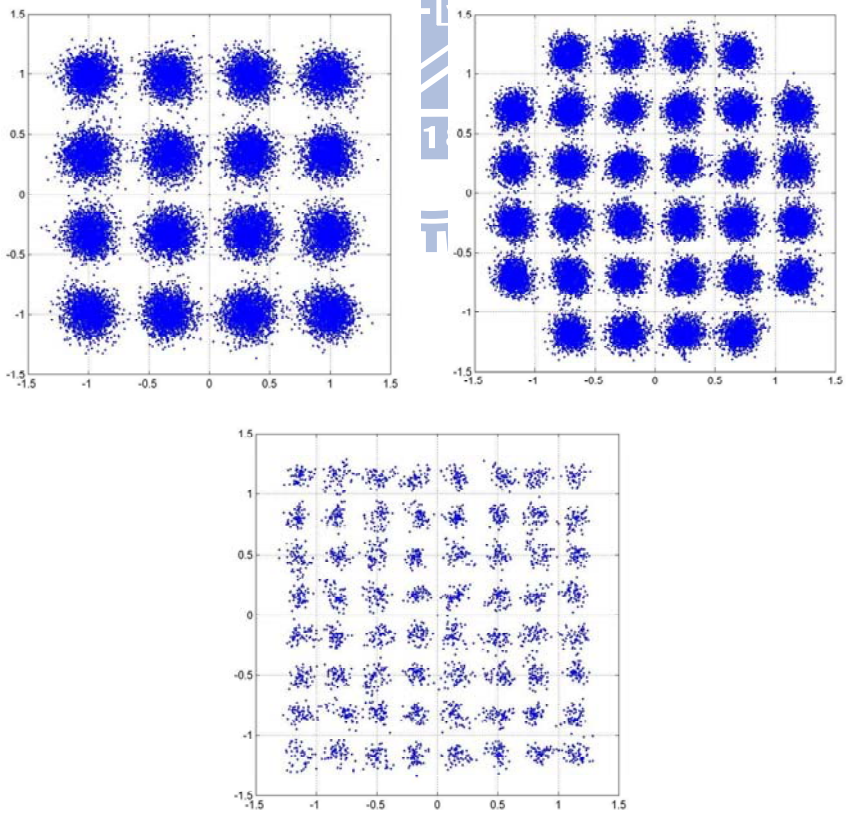

Figure 5-10 (a) BTB Constellation for Bit-loading OFDM signal with wireless transmission.

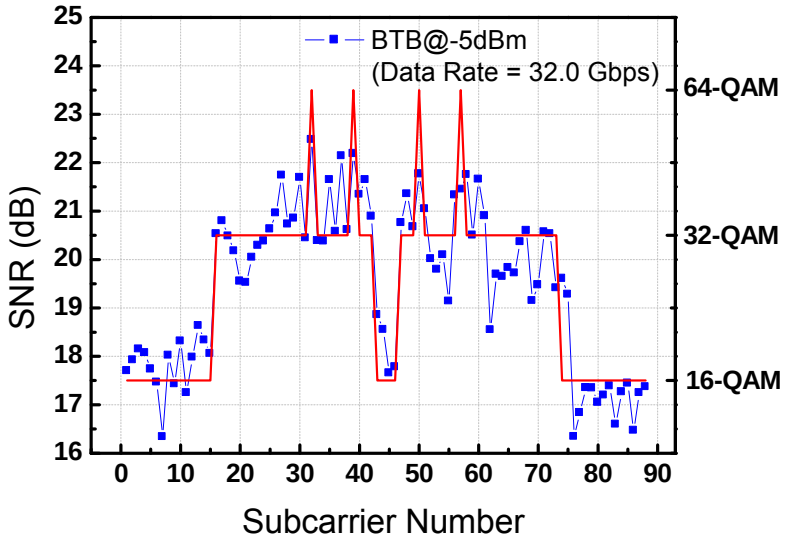


Figure 5-10 (b) BTB SNR vs. Subcarrier Number for Bit-loading OFDM signal with wireless transmission.

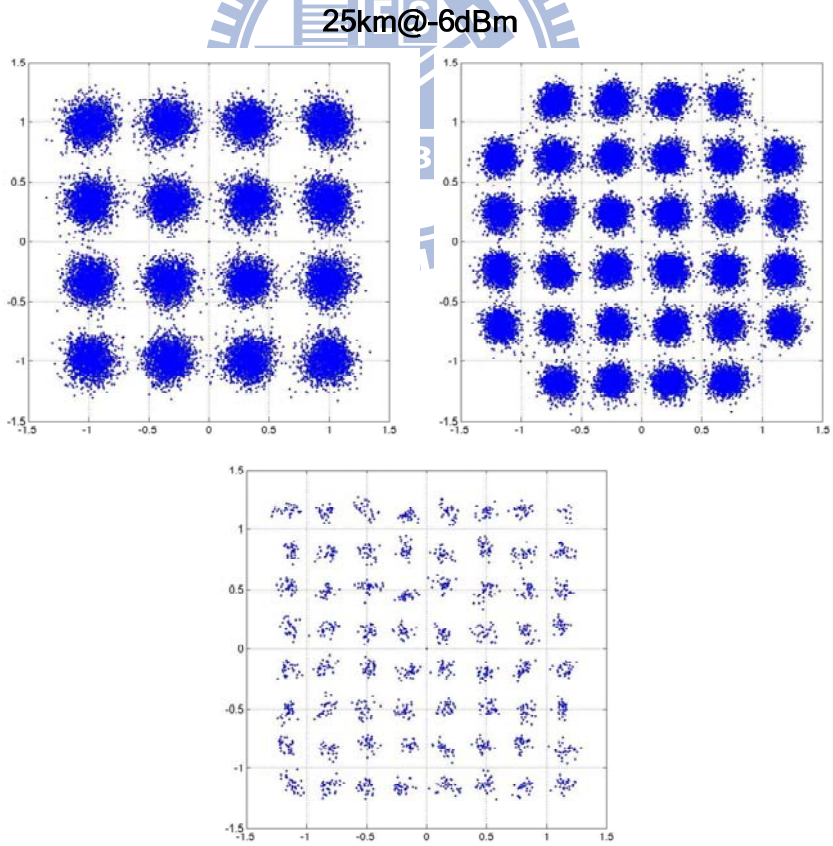


Figure 5-11 (a) Constellation for 25km of Bit-loading OFDM signal with wireless transmission.

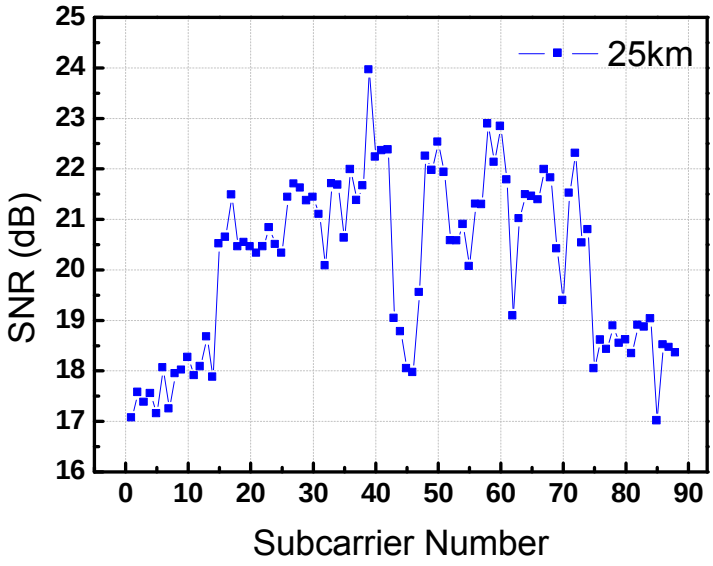


Figure 5-11 (b) SNR vs. Subcarrier Number for 25km of Bit-loading OFDM signal fiber with wireless transmission.

Figure 5-10 shows 32-QAM constellation diagrams and Fig. 5-11 shows SNR vs. subcarrier number after the system in back-to-back and 25km SMF transmission. They are captured at PD received power equal to -8dBm.

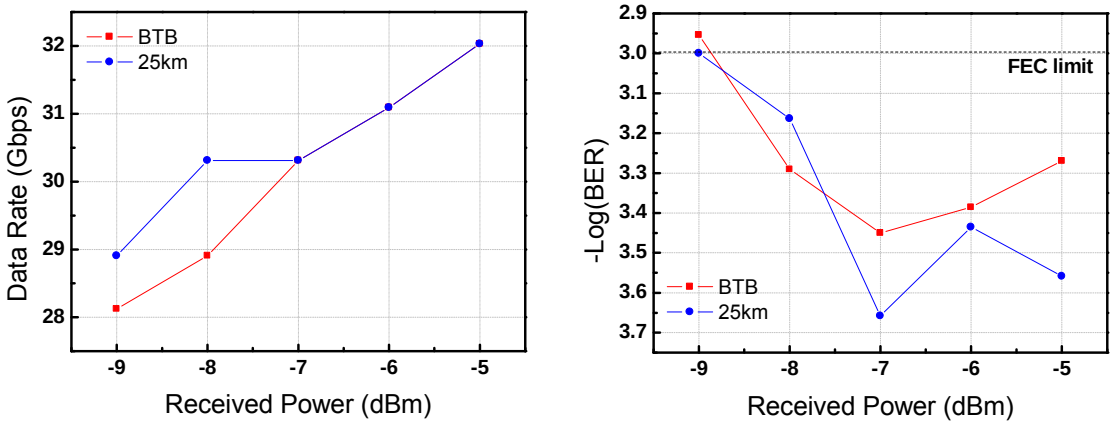


Figure 5-12 (a) Data rate vs. received power of BER below then $10^{-3}$.

| Fiber Transmission = BTB | | |
|---|---|---|
| | | |
| Received Power (dBm) | Data rate (Gbit/sec) | BER |
| -5 | 32.0 | 5.37E-04 |
| -6 | 31.1 | 4.12E-04 |
| -7 | 30.3 | 3.55E-04 |
| -8 | 28.9 | 5.12E-04 |
| -9 | 28.1 | 0.00111 |

| Fiber Transmission = 25km | | |
|---|---|---|
| | | |
| Received Power (dBm) | Data rate (Gbit/sec) | BER |
| -5 | 32.0 | 2.76E-04 |
| -6 | 31.1 | 3.67E-04 |
| -7 | 30.3 | 2.20E-04 |
| -8 | 30.3 | 6.86E-04 |
| -9 | 28.9 | 1.00E-03 |

Figure 5-12 (b) Fixed BER of each received power below then $10^{-3}$.

Figure 5-12 shows data rate and BER vs. received power after the system in back-to-back and 25km SMF transmission. We fixed BER of each point below then $10^{-3}$. They have different data throughput of received power.

# Chapter 6

## Conclusion

Bit-loading algorithms that have high system throughput while guaranteeing a mean BER below a given target value for multicarrier systems are presented. Results showed that the bit-loading algorithm could be used to optimize the signal and increase performance of system to achieve higher data rate, even the channel response have non-flat channel response, especially for 60 GHz RoF system with up to 10 dB deviation within the 7 GHz spectrum. This algorithm provides a solution that can satisfy the demand of 60GHz application within 7GHz license-free band.

Bit-loading algorithm significantly improves performance and data throughput of ultra-wideband mm-wave RoF systems, it has a great potential to allocate appropriate modulation format for each subcarriers. As the results, we used bit-loading algorithm to optimize OFDM signals at different received power and record 32Gbps 25km fiber transmission on 3m wireless distance was achieved. We demonstrate the dynamic OFDM modulation in 60GHz RoF system.

# REFERENCES


[1] Report of the Unlicensed Devices and Experimental Licenses Working Group, Federal Communications Commission Spectrum Policy Task Force, 15th November 2002.

[2] Amendment of Part 2 of the Commission's Rules to Allocate Additional Spectrum to the Inter-Satellite, Fixed, and Mobile Services and to Permit Unlicensed Devices to Use Certain Segments in the 50.2-50.4 GHz and 51.4- 71.0 GHz Bands, FCC 00-442, Federal Communications Commission, December2000.

[3] A. J. Lowery and J. Armstrong, "Orthogonal-frequency-division multiplexing for dispersion compensation of long-haul optical systems," Opt. Express 14, 2079-2084 (2006).

[4] I. B. Djordjevic and B. Vasic, "Orthogonal frequency division multiplexing for high-speed optical transmission," Opt. Express 14, 3767-3775 (2006).

[5] H. Bao and W. Shieh, "Transmission simulation of coherent optical OFDM signals in WDM systems," Opt. Express 15, 4410-4418 (2007).

[6] W. H. Chen, and W. I. Way, "Multichannel Single-Sideband SCM/DWDM Transmission System," J. Lightwave Technol 22, 1697-1693 (2004).

[7] C. Wu, and X. Zhang, "Impact of Nonlinear Distortion in Radio Over Fiber Systems with Single-Sideband and Tandem Single-Sideband Subcarrier Modulations," J. Lightwave Technol. 24, 2076-2090 (2006).

[8] T. N. Duong et al., "Adaptive Loading Algorithm Implemented in AMOOFDM for NG-PON System Integrating Cost-Effective and Low-Bandwidth Optical Devices" IEEE PTL 21, 790-792 (2009).

[9] J. Armstrong and S. Member, “OFDM for Optical Communications,” J. Lightwave Technol. vol. 27, no. 3, FEBRUARY 1, 2009

[10] Lin, Y. Demonstration and design of high spectral efficiency 4Gb/s OFDM system in passive optical networks. 2007.

[11] J. M. Tang and K. Alan Shore, “30-Gb/s signal transmission over 40-km directly modulated DFB-laser-based single mode fiber links without optical amplification and dispersion compensation,” J. Lightw. Technol., vol. 24, no. 6, pp. 2318–2326, Jun. 2006.

[12] J. M. Cioffi, Digital Communication. Stanford University: Lecture Notes, 2004.

[13] J. R. Barry, E. A. Lee, and D. G. Messerschmitt, Digital Communication, 3rd ed. Norwell, MA, USA: Kluwer Academic, 2004.

[14] G. Ana, “SNR Gap Approximation for M-PSK-Based Bit Loading,” TWC, vol. 5, no. 1, Jun 2006

[15] A. Peled and A. Ruiz, “Frequency domain data transmission using reduced computational complexity algorithms,” in Proc. ICASSP 80, Denver, CO, USA, 1980, vol. III, pp. 964–967, IEEE.

[16] J. Park, W. V. Sorin and K. Y. Lau “Elimination of the fiber chromatic dispersion penalty on 1550 nm millimeter-wave optical transmission,” Electron. Lett., vol. 33, pp. 512, 1997.

[17] J. L. Corral, J. Marti, and J. M. Fuster, “General Expressions for IM/DD Dispersive Analog Optical Links with External Modulation or Optical Up-Conversion in a Mach–Zender Electrooptical Modulator,” IEEE Trans. Microwave Theory Tech., vol. 49, pp. 1968–1976, Oct. 2001.

[18] Q. Chang, H. Fu, and Y. Su, “A Radio over Fiber System for Simultaneous Generation and Transmission of Multiband Signals”, IEEE Photon. Technol. Lett., vol. 20, pp. 181-183, 2008.

[19] Z. Xu, X. Zhang, and J. Yu , “Frequency upconversion of multiple RF signals using optical carrier suppression for radio over fiber downlinks”, Opt. Express, vol. 15, pp. 16737-16747, 2007.